NEDO-21983
79NED79
CLASS I
SEPTEMBER 1979

MARK I CONTAINMENT PROGRAM SUBMERGED STRUCTURES MODEL MAIN VENT AIR DISCHARGES EVALUATION REPORT

TASK NUMBER 5.14.1

S. L. LIU
L. E. LASHER

GENERAL ELECTRIC

NEDO-21983
79NED79
Class I
September 1979

MARK I CONTAINMENT PROGRAM

SUBMERGED STRUCTURES MODEL MAIN VENT AIR DISCHARGES EVALUATION REPORT

Task 5.14.1

S. L. Liu
L. E. Lasher

Reviewed by: H E Townsend
H. E. Townsend, Manager
Containment Methods

Approved by: A. E. Rogers
A. E. Rogers, Manager
Containment Technology

Approved by: A E Rogers for
E. Kiss, Manager
Applied Mechanics

NUCLEAR ENGINEERING DIVISON • GENERAL ELECTRIC COMPANY
SAN JOSE, CALIFORNIA 95125

GENERAL ELECTRIC

DISCLAIMER OF RESPONSIBILITY

Neither the General Electric Company nor any of the contributors to this document makes any warranty or representation (express or implied) with respect to the accuracy, completeness, or usefulness of the information contained in this document or that the use of such information may not infringe privately owned rights; nor do they assume any responsibility for liability or damage of any kind which may result from the use of any of the information contained in this document.

TABLE OF CONTENTS

LIST OF ILLUSTRATIONS

LIST OF ILLUSTRATIONS (Continued)

1764 052

LIST OF ILLUSTRATIONS (Continued)

1764 053

LIST OF TABLES

ABSTRACT

Predictions of the analytical model for estimating drag loads on submerged structures by main vent air discharges following a postulated loss-of-coolant accident are compared to the results obtained from the one-quarter scale Mark I submerged structure test program.

Results of the one-quarter scale Mark I submerged structure experiment show that the analytical model grossly overpredicts loads in a scaled prototypical Mark I facility. Alternate modeling is evaluated which gives more reasonable, but still conservative predictions. The quarter-scale experiment also verifies the uniform flow assumption of the analytical model.

1. INTRODUCTION

1.1 PHENOMENA DESCRIPTION

The phenomena considered in this model evaluation report are concerned with the sequence of events that occur following a postulated loss-of-coolant accident (LOCA). During the initial phase of the design-basis accident (DBA), pressurized drywell air is purged into the wetwell suppression pool through submerged downcomer vents. Right after vent clearing (clearing of the downcomer water column), a bubble is formed at each vent exit. The bubble expands due to lower pool pressure and continued air charging from the drywell. The charging LOCA bubbles from the downcomer exits displace the surrounding pool water and cause the pool-swell phenomenon in the wetwell. It is during this bubble growth period, i.e., the time from which the bubble is initially formed to the time of the bubble breakthrough of the swelling pool surface, that unsteady three-dimensional fluid motion is created within the suppression pool. Consequently, all submerged structures below the pool surface will react to the hydrodynamic loads imposed upon them by the unsteady bulk fluid motion.

The duration of the LOCA bubble is short (for example, in a Mark I plant the time from initial formation to break-through of the pool surface for a 4 ft. downcomer submergence is typically on the order of 0.6 second for the DBA). Loading on submerged structures results from the unsteady velocity and acceleration flow fields within an initially stagnant pool that are created by the charging bubbles.

1.2 BRIEF DESCRIPTION OF ANALYTICAL MODEL

Immediately following a postulated LOCA, an air bubble forms at the main vent exit displacing the water in the surrounding region. The resulting velocity and acceleration fields in the suppression pool cause loads on submerged structures. The velocity field imposes form drag loads that are proportional to the local velocity squared; the acceleration field imposes an acceleration drag load that is proportional to the local acceleration.

The algebraic sum of these forces, form drag plus acceleration drag, gives the total drag on a submerged structure. The form and acceleration drag forces at any point in the suppression pool are computed from the local velocity and acceleration, respectively.

The formulation of the analytical model (Reference 1) is based on the analysis of structures that are submerged in a locally uniform flow field. Actual flow fields in a water pool are characterized by curved streamlines, which depend upon the actual geometry. The fluid velocity and acceleration vectors, therefore, are functions of both space and time. The drag due to the flow field is postulated to be equal to the drag calculated in a uniform flow with the velocity and acceleration evaluated at the geometric center of the structures. The flow field is computed as being created from an expanding spherical gas bubble.

The bubble dynamics utilized in the model are assumed to be governed by the Rayleigh equation (Reference 2). The bubble pressure is obtained from a combination of thermodynamic and kinematic considerations. The model first calculates the bubble dynamics for a bubble in an infinite pool. The results are then adjusted using the method of images to account for the presence of solid walls and the free surface. In addition, a factor is introduced to satisfy the local pressure boundary condition at the bubble surface.

1.3 TEST PROGRAM DESCRIPTION

As part of the submerged structures program, a Mark I 1/4-scale test program was developed. The Mark I 1/4-scale submerged structure test program (Reference 3) consisted of eight tests performed at the 1/4-scale test facility at Acurex/Aerotherm.

The main objective of the Mark I 1/4-scale test program was to show that the load prediction methods of the analytical model (Reference 1), when applied to the calculated flow fields, conservatively predict loads occurring during the main vent air bubble expansion in a scaled prototypical Mark I facility. Additional objectives were to confirm the assumption that the uniform flow procedure holds for targets of different effective proximities to the air bubble, and to assess the effect on submerged structure loads under the full drywell initial overpressure condition.

2. ANALYTICAL MODEL

When air discharge occurs in a suppression pool due to a postulated loss-of-coolant accident, velocity and acceleration fields are established which create drag forces on submerged structural members. The velocity field imposes a velocity squared standard drag force, whereas the acceleration field imposes an additional component called the acceleration drag force. To ensure that the mechanical design of the affected structural members is adequate, the total in-line force, which is composed of both standard and acceleration drag, must be estimated. The complete description of the model is given in Reference 1.

2.1 MAJOR ASSUMPTIONS

1. The total drag is the sum of standard and acceleration drags;

2. The air bubble is spherical, with the flow field being described by a point source;

3. The flow field around submerged structures can be represented by a locally uniform flow field;

4. The presence of boundaries, including the free surface, can be incorporated by using the method of images;

5. Air is assumed to be an ideal gas, and the flow through the vents is assumed to be isentropic;

6. The initial LOCA bubble pressure is assumed to be the maximum dry-well value before breakthrough;

7. Acoustic wave propagation effects are small compared to the bulk water motion in the system.

2.2 AIR BUBBLE FORMATION LOADS

Initially, the bubble center is located on the downcomer axis at a distance equal to the downcomer radius below the downcomer exit, and the bubble center is assumed to remain at this location throughout the charging transient. The bubble-dynamics equations along with the bubble-charging equations are given in Reference 1. Employing the appropriate initial conditions for the LOCA air bubble, as described in Reference 1, this coupled set of equations may be solved for:

$R(t)$ = The bubble radius at time t

$\dot{R}(t)$ = The bubble growth rate at time t

$\ddot{R}(t)$ = The rate of change of the bubble growth rate with respect to time at time t.

To determine the distance between bubble and submerged structure, the following dimensions are noted:

r_o = The distance from the bubble center to the center of the structure, and

D_s = The structure cross-section dimension in the direction of r_o.

These values are then compared to R(t) to check whether there has been structure/bubble contact, i.e., is $R(t) \geq (r_o - D_s/2)$? If true, the loading calculations end because the structure is partially or fully inside the air bubble and the drag forces are insignificant.

To account for the wall and free surface effects, all the image sources and sinks for the bubble are located as described in Section 4.10 in Reference 1. The factor K included in function X, Y, and Z (as given in Equation A 67 of Reference 1) accounts for finite bubbles effects.

1764 060

where:

X, Y, and Z = Constants determined from bubble, structure, and confining geometry

K = Factor for finite bubble size.

The direction of the drag force at time t can be determined by the following equation:

$$\vec{n} = \frac{X\,\vec{n}_x + Y\,\vec{n}_y + Z\,\vec{n}_z}{\sqrt{X^2 + Y^2 + Z^2}} \qquad (2\text{-}1)$$

where:

$\vec{n}$ = Unit vector of drag force

$\vec{n}_x, \vec{n}_y, \vec{n}_z$ = Unit vectors in the X,Y,Z directions, respectively.

The equivalent uniform acceleration field at time t is given by:

$$\dot{U}_\infty(t) = (R^2(t)\,\ddot{R}(t) + 2R(t)\,\dot{R}^2(t))\,\sqrt{X^2 + Y^2 + Z^2} \qquad (2\text{-}2)$$

$U_\infty(t)$ is obtained by numerically integrating $\dot{U}_\infty(t)$.

where:

$\dot{U}_\infty(t)$, $U_\infty(t)$ = Equivalent uniform flow acceleration and velocity, respectively.

The components normal to the structure are:

$$U_{\infty N}(t) = U_\infty(t) \cos\theta \qquad (2\text{-}3)$$

$$\dot{U}_{\infty N}(t) = \dot{U}_\infty(t) \cos\theta \qquad (2\text{-}4)$$

1764 061

where θ is the angle between $\vec{n}$ and the inward normal to the structure.

The acceleration drag is calculated using

$$F_A(t) = \frac{\dot{U}_{\infty N}(t)\ V_A \rho}{g_c} \tag{2-5}$$

where ρ = liquid density, g_c = acceleration constant, V_A is the acceleration drag volume (from Tables 1 and 2, Reference 1) for flow normal to the structure. This approach using the normal velocity component is justified in the discussion on "Skewed Structures" in Reference 1. Similarly, the standard drag force is calculated using

$$F_S(t) = C_D\ A_x\ \frac{U^2_{\infty N}(t)}{2g_c}\ \rho \tag{2-6}$$

where C_D is the drag coefficient for flow normal to the structure obtained from Table 3, Reference 1 and A_x is the projected structure area normal to $U_{\infty N}(t)$. The total drag force normal to the structure is then the sum of the standard and acceleration drag forces given above. The drag force tangential to the structure is ignored because it results in relatively small skin friction drag loads.

3. MODEL/DATA EVALUATION

The Mark I 1/4-scale test program was conducted to acquire quantitative total drag loading data on cylindrical targets exposed to a prototypical flow condition generated by the main vent charging air bubbles.

In this section, brief description of the test program and the comparison of the test results with the predictions of the analytical model are presented.

3.1 TEST OBJECTIVE

One of the primary objectives of the 1/4-scale test program was to compare the submerged structure loads predicted by the analytical model due to the LOCA air bubble (Ref. 1) to the actual loads measured in the Mark I 1/4-scale test facility (QSTF).

Other objectives were:

1) To show that the uniform flow assumption is valid at least over the range of D/R from:

$$D/R \leq 0.5$$

where D is the diameter of a representative target and R is the distance between the bubble center and the target center.

2) To assess the effect of submerged structure loads to drywell/wetwell ΔP.

3.2 FACILITY DESCRIPTION

A schematic of the QSTF is shown in Figure 3-1. The 1/4 scale configuratic is based upon a typical Mark I BWR pressure suppression containment. For a detailed description of this facility refer to the 1/4 scale test report (Reference 3).

In order to meet the objectives of the test program, four cylindrical targets designated as A, B, C, D (Figure 3-2) were mounted within the QSTF to determine the submerged structure loads under two simulated LOCA conditions (0" ΔP and 10" ΔP). The targets A, B and C were 10-inch long rigid cylindrical bodies, mounted horizontally across the width of the QSTF in cantilever supported by individual flexible beam tubes. The target D was a cylinder, 54.0 inches long and 1.66 inches o.d., mounted vertically between the QSTF vent header and the torus bottom, with the size simulating the vent header support column in a typical Mark I containment design.

Strain gages were positioned on all targets to register the combination of instantaneous fluid drag loads and the inertial loads induced by support structures and motion of the facility. Accelerometers, to be used for the determination of inertial force, were installed in targets A, B, and C. A high-speed movie camera was used at 500 frames per second to film the blow-down event for each test condition. Films were analyzed to determine the water clearing process and the flow-field generated by the blowdown throughout the whole transient.

3.3 LOAD EVALUATION

TEST-DATA REDUCTION

All strain gage and accelerometer test data, in addition to the required facility measurements, were recorded. Software programs to convert the raw data into appropriate engineering units were developed. In order to properly evaluate the measured loads, the structure base reference movements from the vibrating facility had to be eliminated. The evaluated test

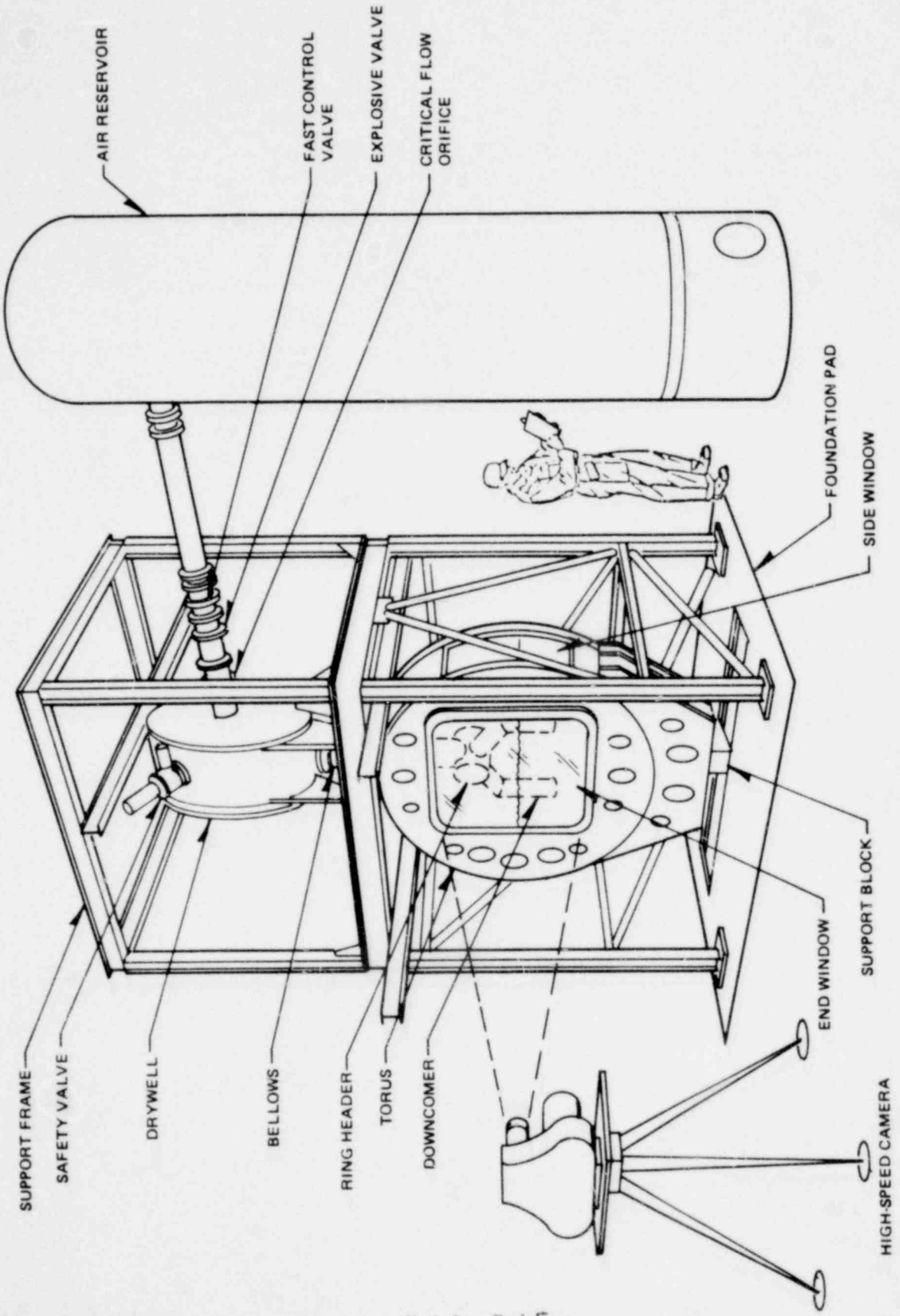

Figure 3-1. Mark I 1/4 Scale Test Facility

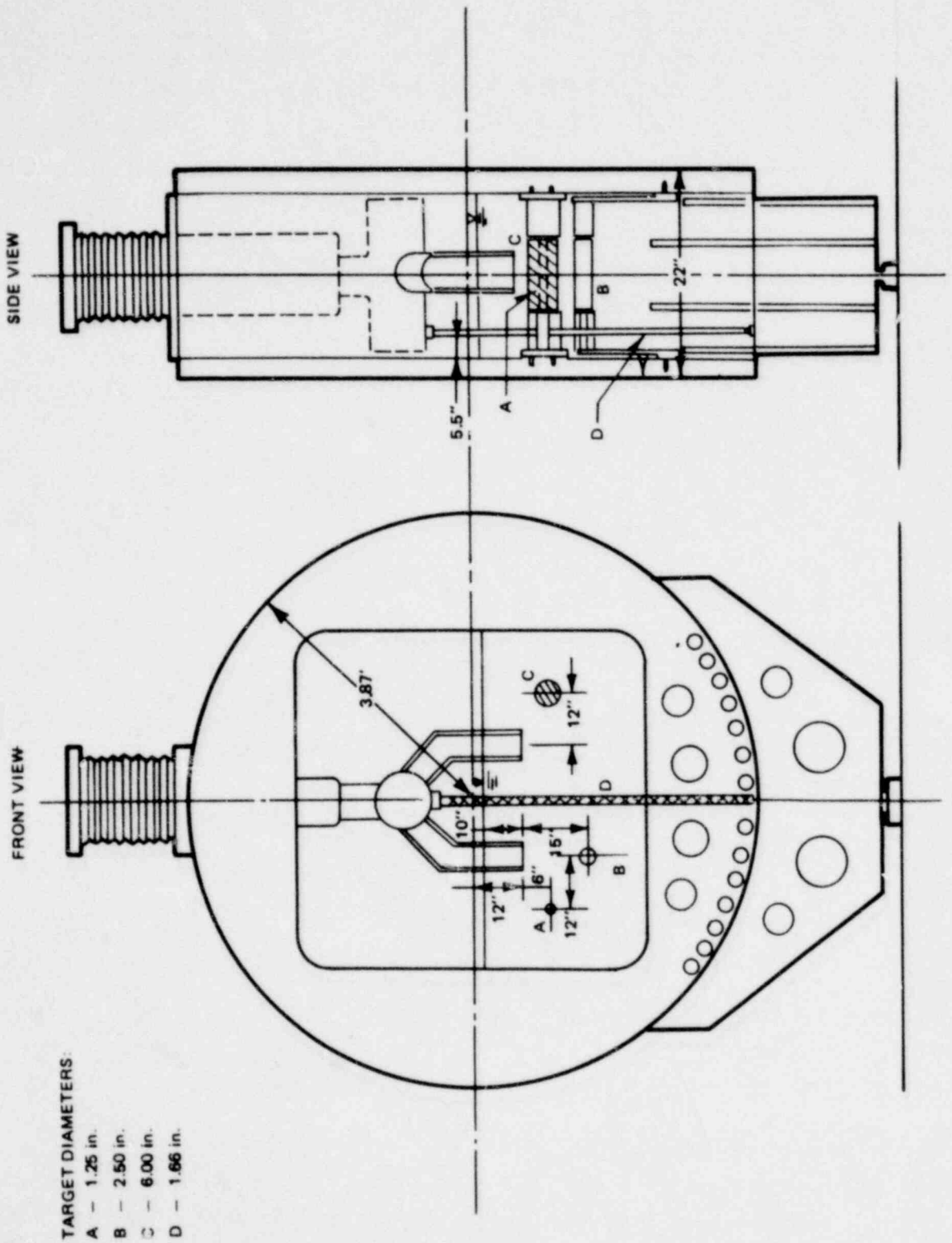

Figure 3-2. Submerged Target Positions in the Mark I 1/4 Scale Test Facility

1764 066

results could then be compared directly to the predicted model results. The model assumes the submerged structures to be rigid bodies. A detailed description of the procedure used to obtain the target time history induced by fluid forces alone is presented in Appendix D of Reference 3.

Figure 3-3 shows typical drywell and two downcomer bubble pressure-time histories. Figures 3-4 and 3-5 show the typical transient fluid force in the vertical and horizontal directions for Targets A, B, and C at $\Delta P = 0$. Figure 3-6 and Figure 3-7 are for the case where $\Delta P = 10"$. Table 3-1 shows the test results for peak force on Targets A, B, and C. Table 3-2 provides vertical target peak loads for target D.

The vent clearing time for $\Delta P = 0$ is determined from the analysis of the recorded high speed film. It is found, when compared with Figure 3-3, that the vent clears about 2 to 3 ms immediately after the point where downcomer bubble pressure coincides with drywell pressure at approximately 7.2 psia. It can also be seen from this figure that the maximum bubble pressure begins to decrease immediately after vent clearing and drywell pressure continues to increase. This is due to increasing gas flow rate into the bubble and development of frictional pressure drop in the vent system.

Analytical Model Prediction

The analytical description for the air bubble loads is given in Section 2.0. The equations required to obtain submerged structure loads have been computerized. The curved pool boundary for image computation is approximated by five equivalent cell models (Table 3-3). The recorded drywell pressure transient curves after vent clearing are approximated by several straight segments as an input parameter to the computer program. The standard drag coefficient, $C_D = 1.2$, is used for the calculation of standard drag force on all targets. The calculation procedure assumes the bubble center is located on the downcomer axis at a distance equal to the downcomer radius below the downcomer exit, and remains at this location throughout the charging transient.

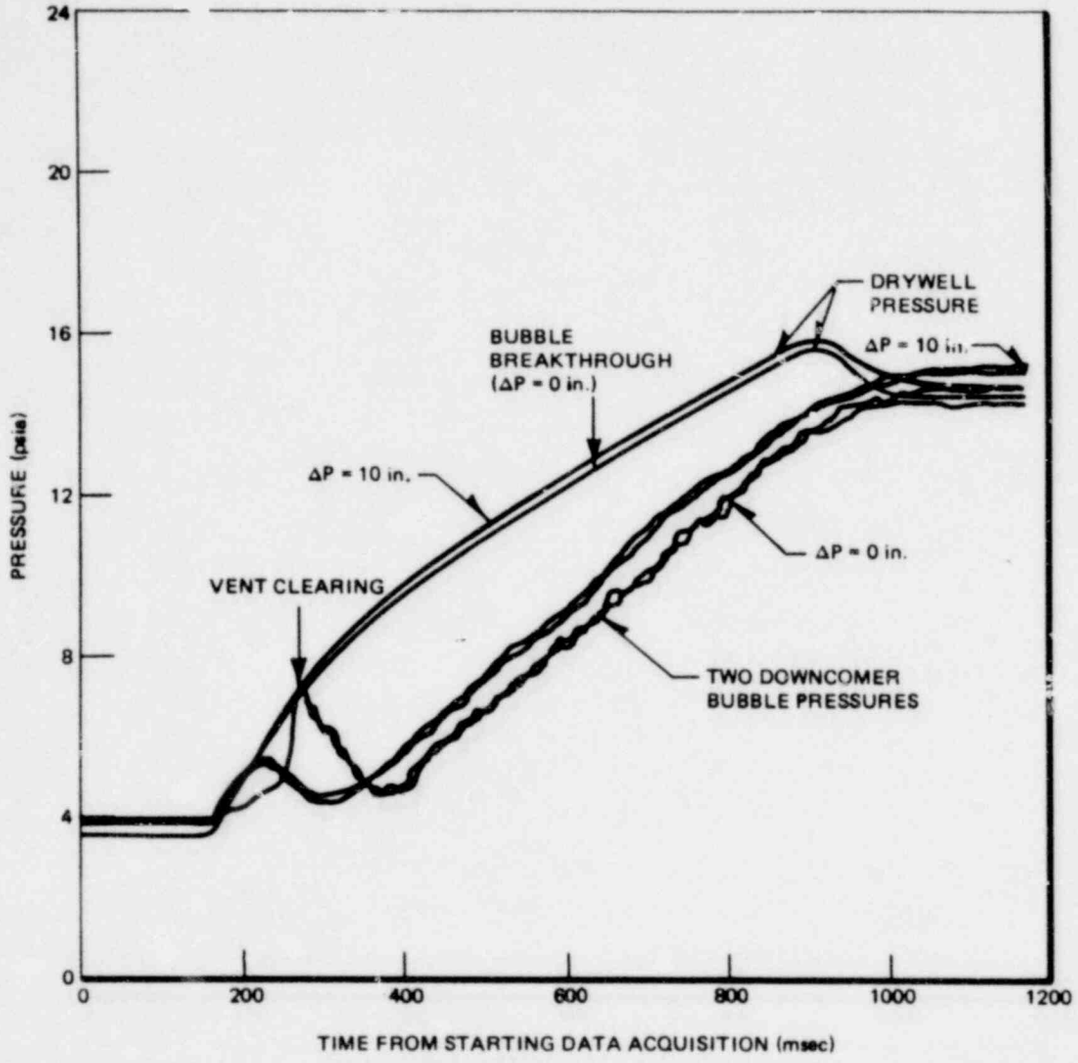

1764 068

Figure 3-3. Typical Drywell and Bubble Pressure Time Histories for ΔP = 0 and 10 in.

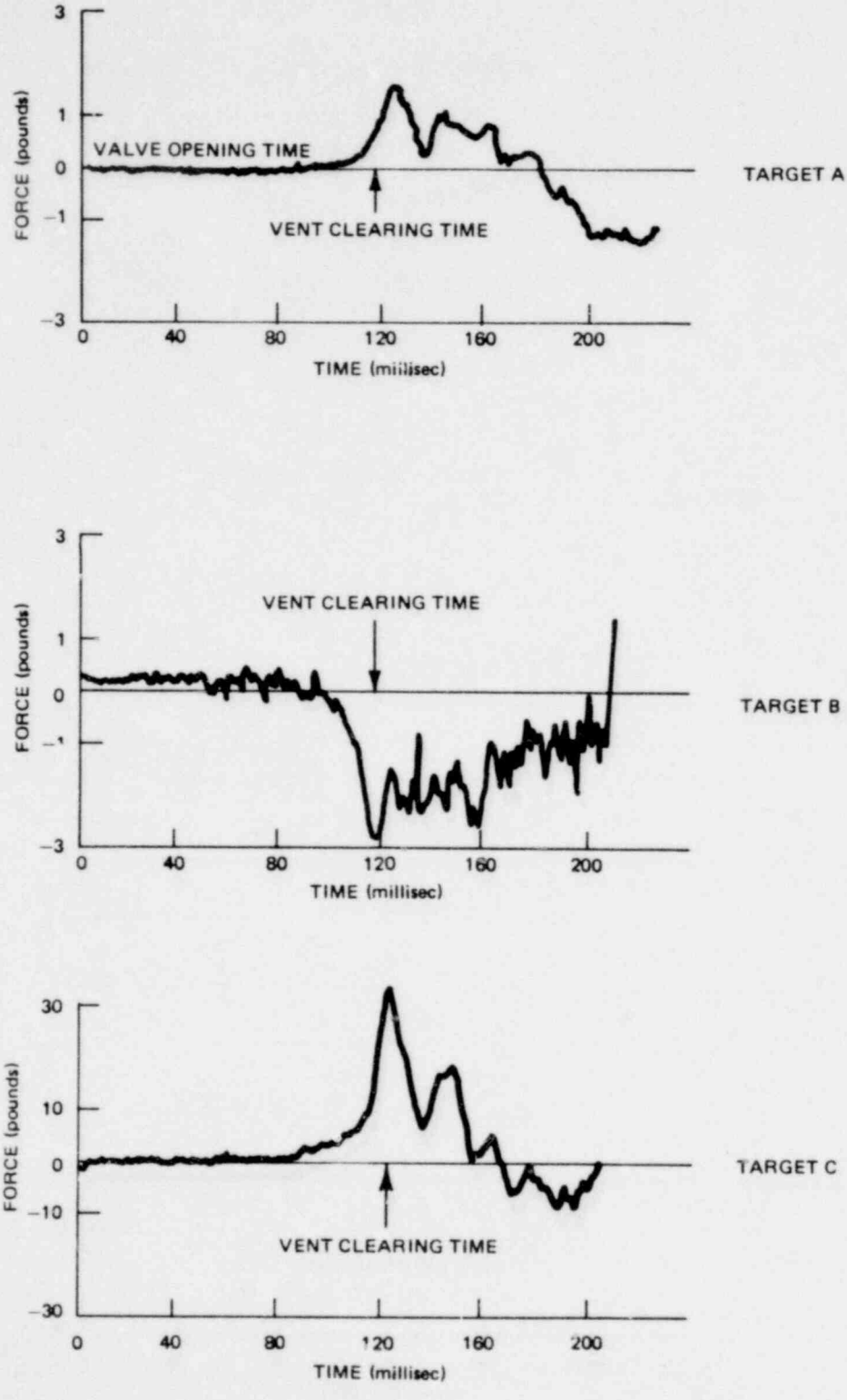

Figure 3-4. Typical Transient Vertical Fluid Force Component on Targets A, B and C ($\Delta P = 0$) (Positive Force is Upward)

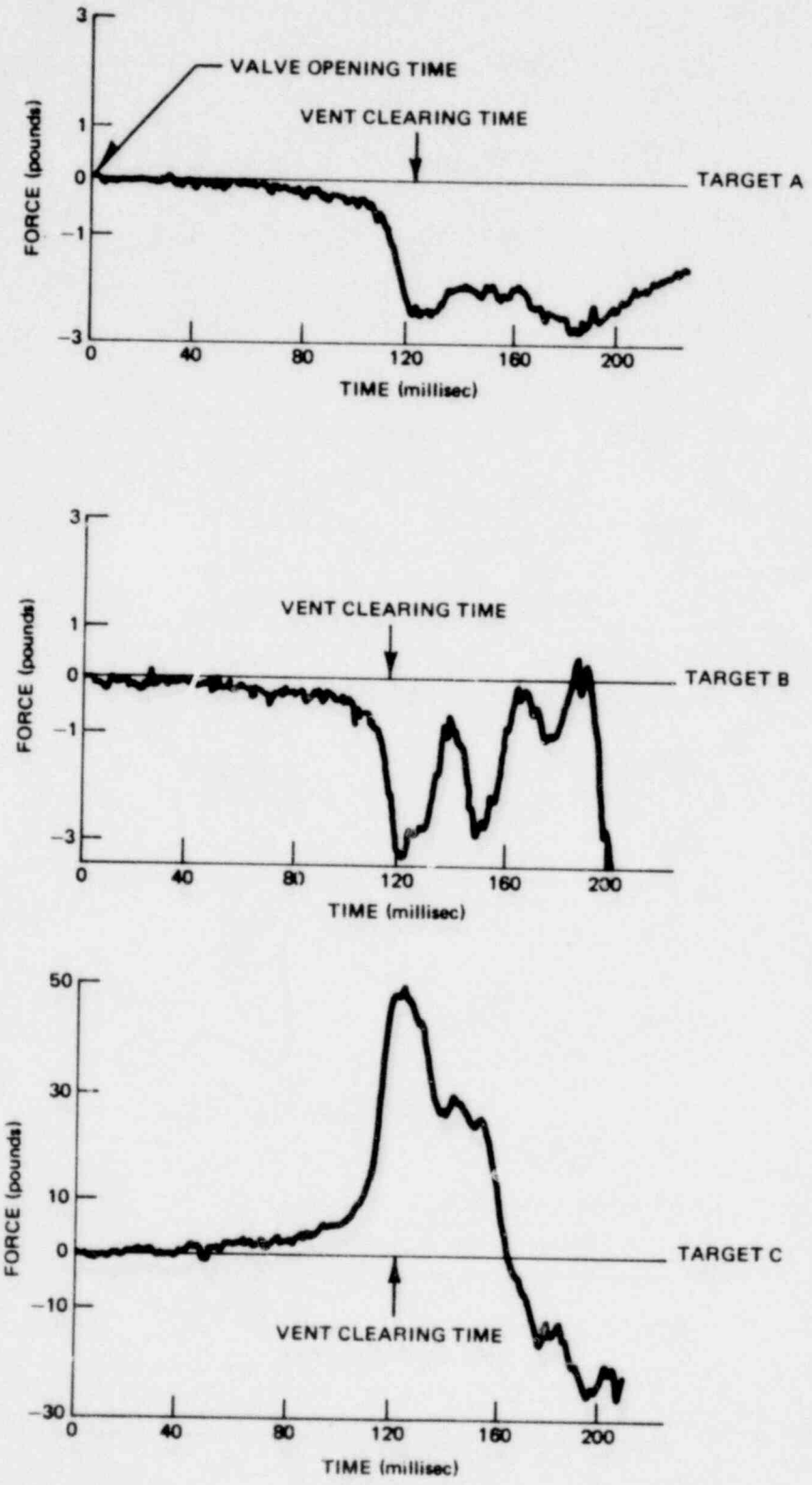

Figure 3-5. Typical Transient Horizontal Fluid Force Component on Targets A, B and C ($\Delta P = 0$) (Positive Force is to the Right From Facility Vertical Centerline)

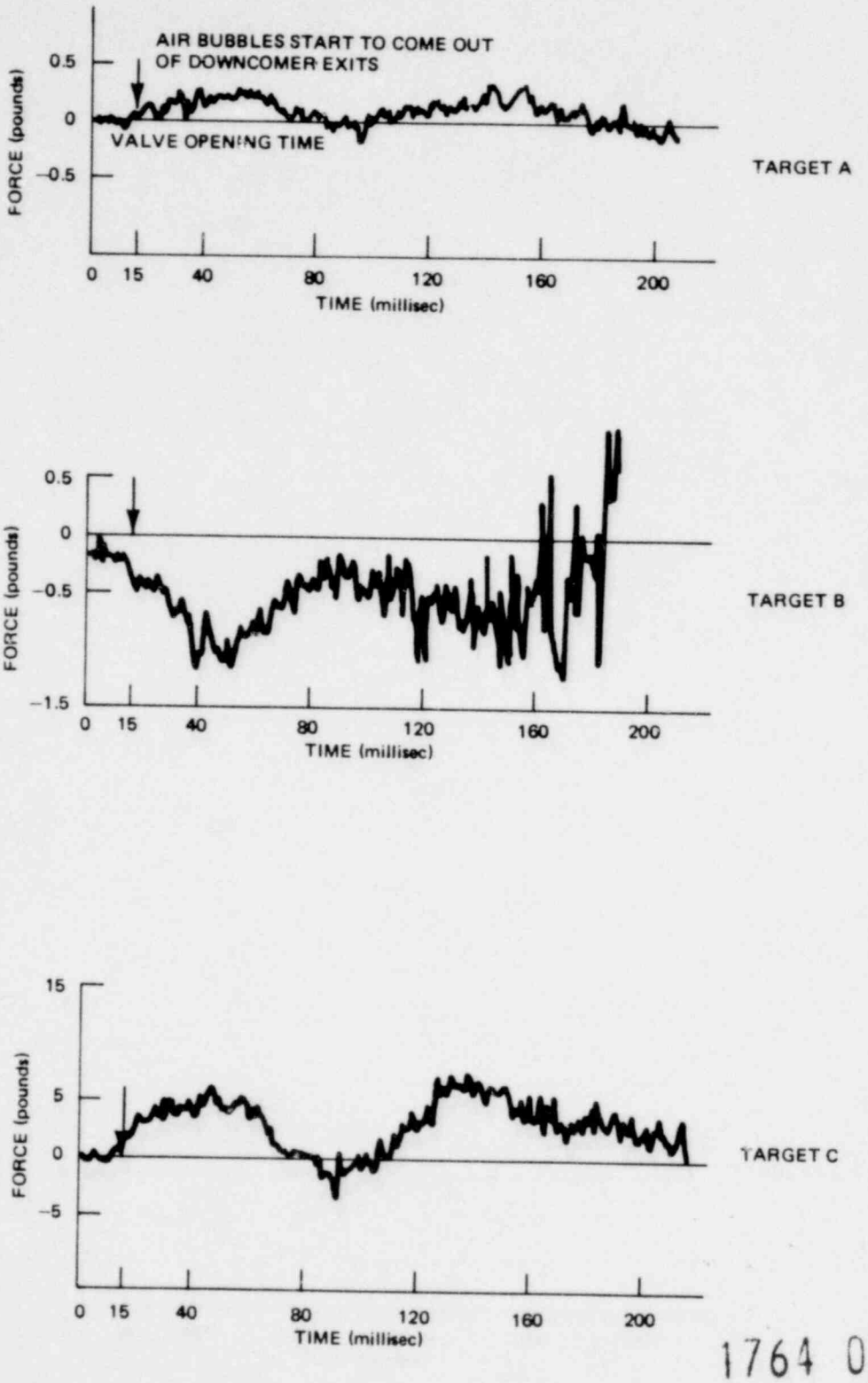

1764 071

Figure 3-6. Typical Transient Vertical Fluid Force Component on Targets A, B, and C (ΔP = 10 in.) (Positive Force is Upward)

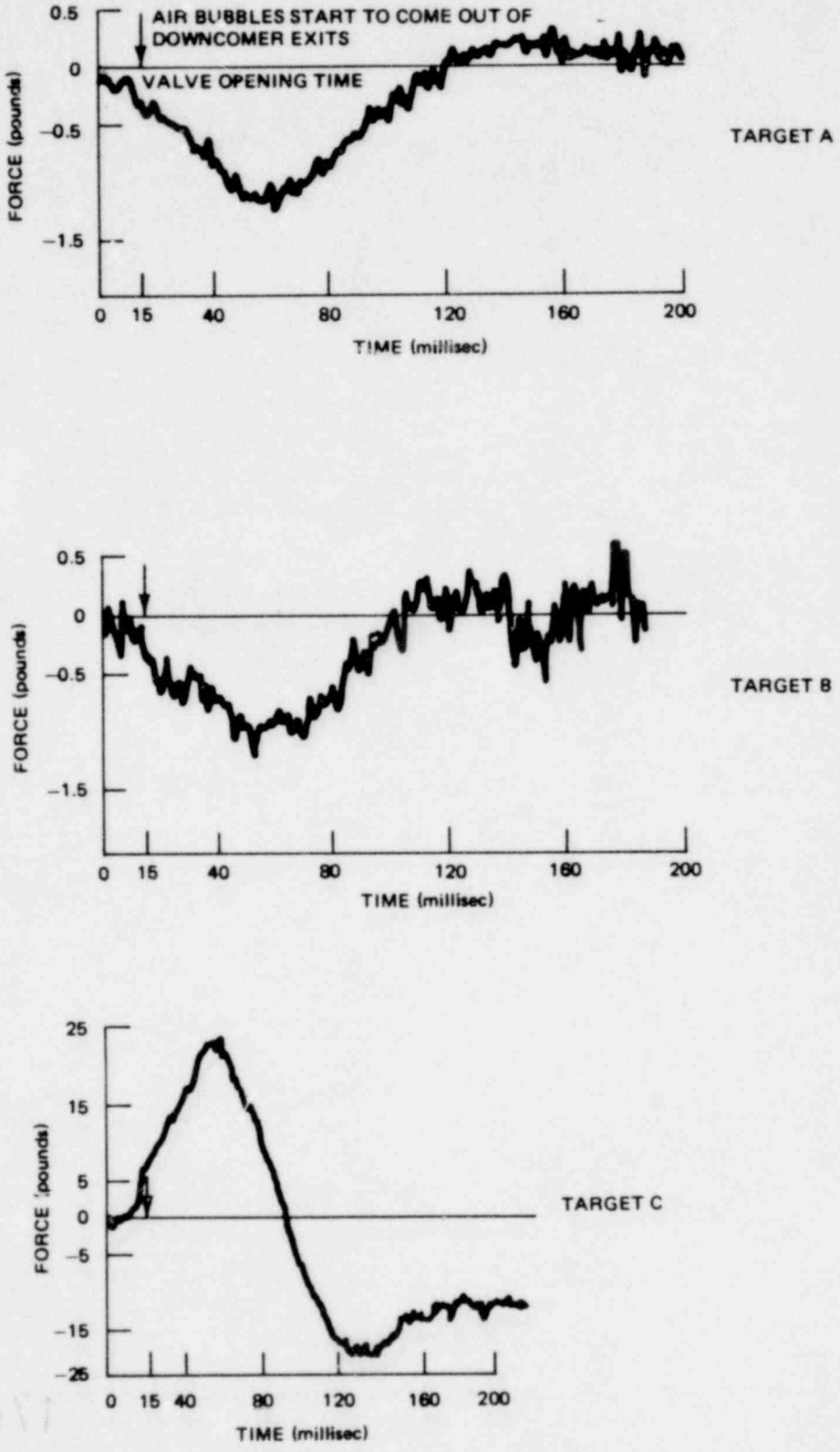

Figure 3-7. Typical Transient Horizontal Fluid Force Component on Targets A, B, and C (ΔP = 10 in.) (Positive Force is to the Right from Facility Vertical Centerline)

Table 3-1

PEAK FORCE ON TARGETS A, B AND C UNDER ΔP = 0 IN. AND ΔP = 10 IN. (Company Proprietary)

ΔP = 0 in. H_2O

Test No.	Target A Vert. (lb)	Target A Hori. (lb)	Target B Vert. (lb)	Target B Hori. (lb)	Target C Vert. (lb)	Target C Hori. (lb)	
ST-1							*
ST-3							
ST-5							
ST-8							
Mean							
σ							
Resultant							
Fluid Force per Unit Area							

$$\frac{\text{Resultant force C}}{\text{Resultant force A}} = 21.14 = (4.6)^2$$

ΔP = 10 in. H_2O

Test No.	Target A Vert. (lb)	Target A Hori. (lb)	Target B Vert. (lb)	Target B Hori. (lb)	Target C Vert. (lb)	Target C Hori. (lb)	
ST-2							*
ST-4							
ST-6							
ST-7							
Mean							
σ							

*Proprietary information deleted.

1764 073

Table 3-1 (Continued) (Company Proprietary)

Test No.	Target A Vert. (lb)	Target A Hori. (lb)	Target B Vert. (lb)	Target B Hori. (lb)	Target C Vert. (lb)	Target C Hori. (lb)
Resultant						
Fluid Force per Unit Area						

*

$$\frac{\text{Resultant Force C}}{\text{Resultant Force A}} = 19.13 = (4.4)^2$$

The ratio of the respective diameters between C and A is 4.8

Table 3-2

PEAK LOADS - VERTICAL TARGET D
(Bounding Values)

ΔP (in. H_2O)	Left/Right Load (psi)	Front/Back Load (psi)
0	0.310	0.502
10	0.289	0.395

*Proprietary information deleted.

1764 074

Table 3-3

SUMMARY OF CELL MODELS

Cell Model	Height (ft)	Width (ft)	Depth (ft)
A	H, 3.7083	$\frac{A}{2H}$, 3.0061	1.8167
B	$\frac{A}{2\ell}$, 3.0361	ℓ, 3.6717	1.8167
C	$\sqrt{A/2}$, 3.3388	$\sqrt{A/2}$, 3.3388	1.8167
D	H, 3.7083	ℓ, 3.6717	1.8167
E	H, 3.7083	L, 3.8714	1.8167
Actual	H, 3.7083	L, 3.8714	1.8167

NOTE:

A = pool water cross-sectional area

H = water level

ℓ = pool width at bubble elevation

L = pool width at initial water surface

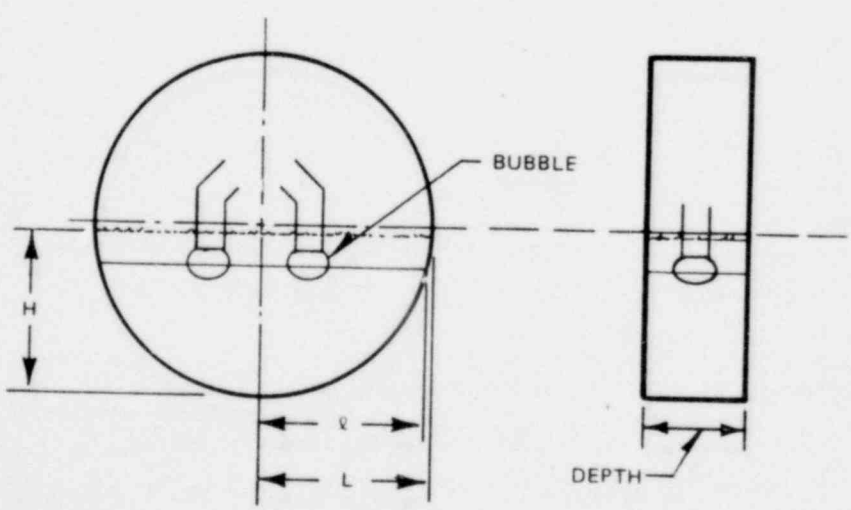

1764 075

Two conditions are used to obtain input for the bubble dynamics: one takes into account varied charging rates, initial bubble wall velocities and overall vent friction; the other follows the procedure specified in the model report (Reference 1) which considers a constant charging rate (use the maximum drywell pressure before breakthrough), a negligible vent friction and zero initial bubble wall velocity. With these later assumptions, the model prediction is expected to be extremely conservative (see Section 3.4).

Figures 3-8 to 3-14 show the predicted values and test results for all targets ($\Delta P = 0$) considering a constant charging pressure of 12.71 psi (i.e., the drywell pressure at time of bubble breakthrough), a zero overall vent friction coefficient (fL/D) and initial bubble wall velocity. Figures 3-15 to 3-28 are the comparison between test results for all targets (both $\Delta P = 0$ and 10 in.) and model predictions based on vent fL/D = 17.6 and the initial bubble wall velocities of 7.5 ft/sec for $\Delta P = 0$" and 0 ft/sec for $\Delta P = 10$". The value of 7.5 ft/sec for $\Delta P = 0$" is obtained from the ratio of bubble surface area to vent cross section area which is 1/4 the measured vent clearing velocity of 30 ft/sec.

3.4 MODEL/DATA COMPARISON

After vent clearing during a postulated LOCA, pressurized drywell air is discharged into the suppression pool through downcomers. The expansion of air bubbles produces a flow field and therefore creates drag forces on submerged structures in the suppression pool. An analytical description to cover the submerged structure load prediction due to LOCA air bubbles is given in Section 2.0. The comparisons between model predictions and test results are presented in Figures 3-8 to 3-28.

Effects of bubble charging rate, vent friction and bubble wall velocity

Predicted loads on targets shown in Figures 3-8 to 3-14 are calculated based on the analytical model considering negligible vent friction, a maximum drywell pressure before breakthrough (rather than much lower values of transient

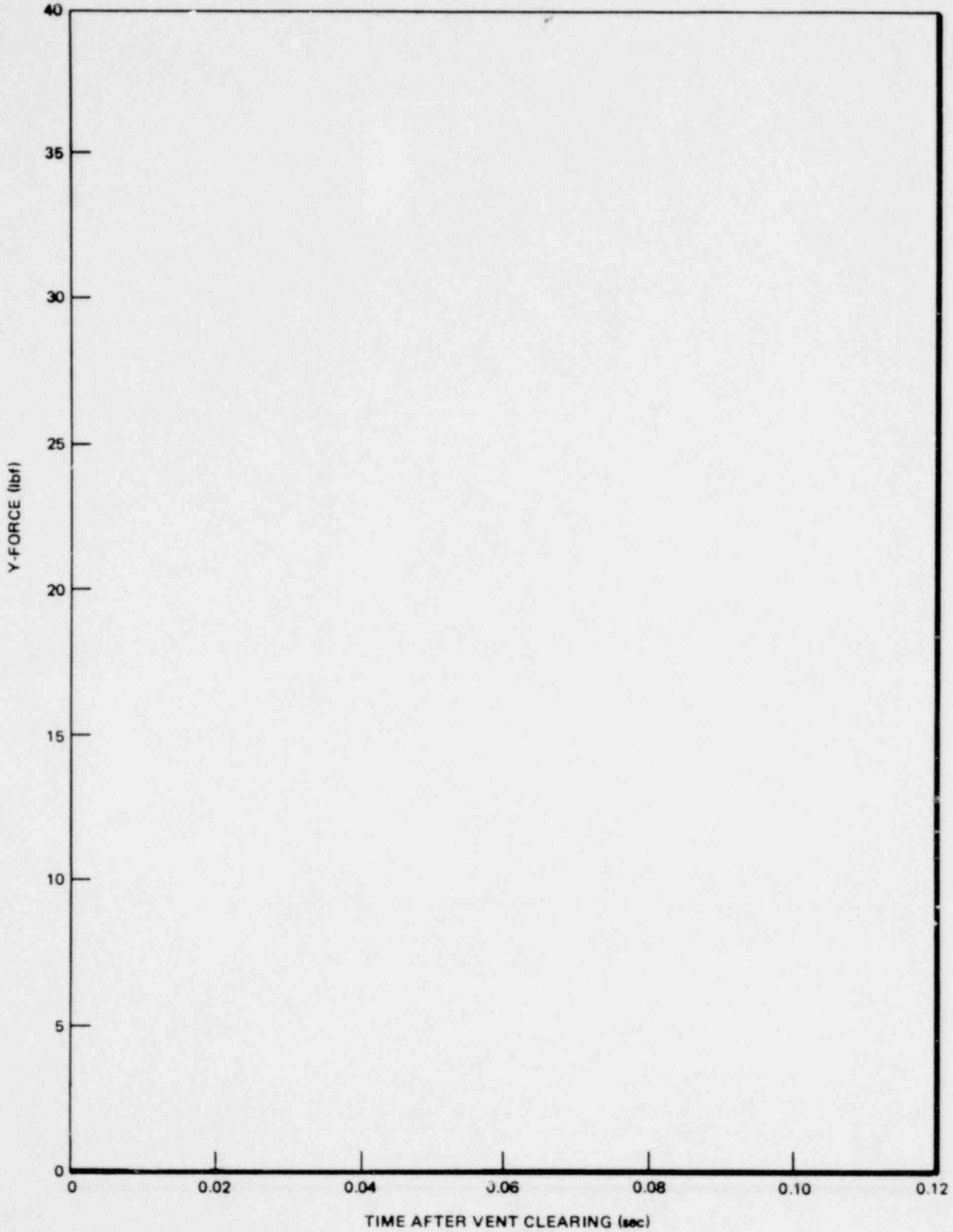

Figure 3-8. Comparison of Predicted Results Using Various Cell Models for Target A in the Vertical Direction With Test Data. Initial Bubble Velocity = 0, FL/D = 0, P_{DW} = 12.71 psi, ΔP = 0

*Proprietary information deleted

1764 077

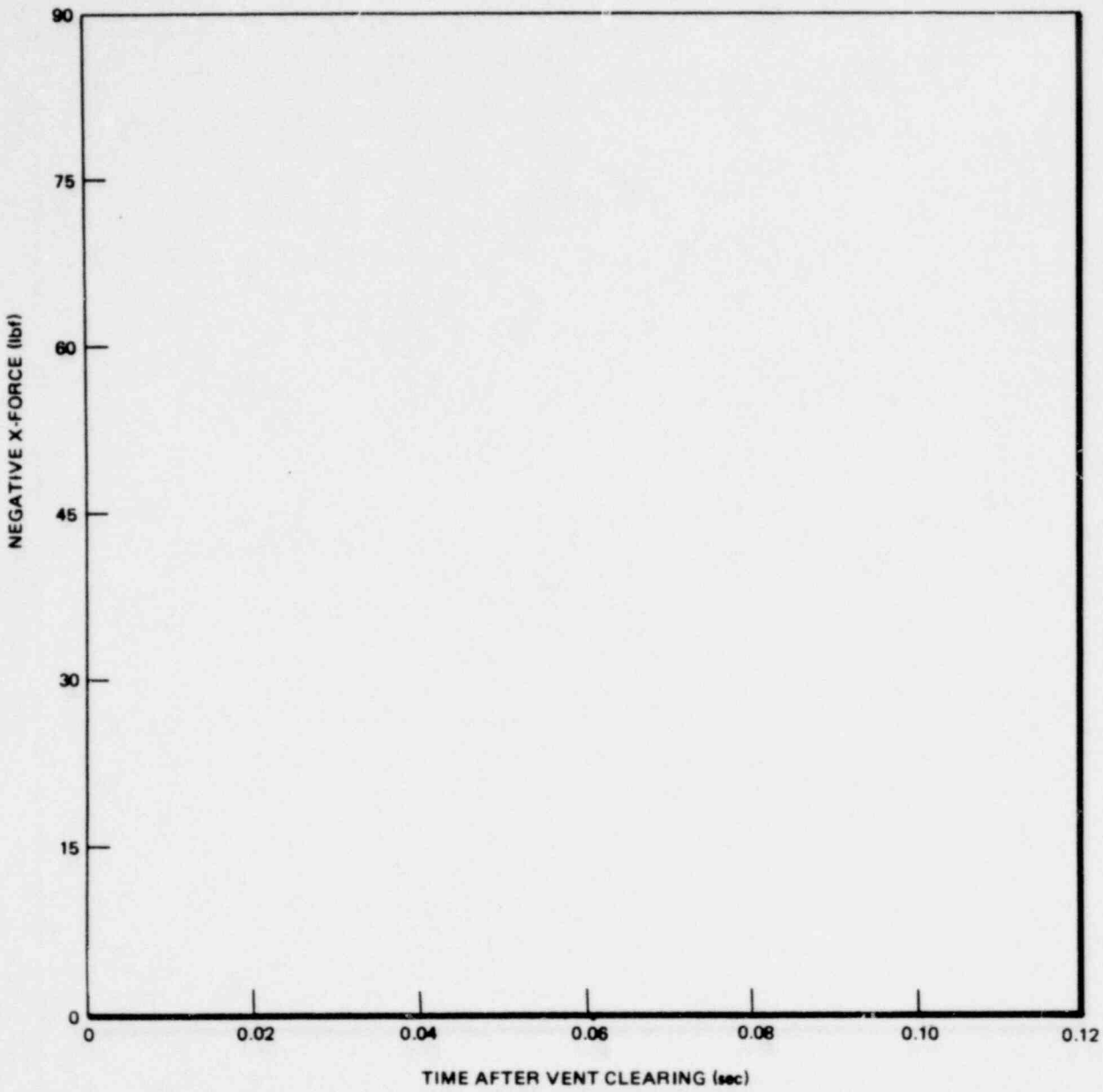

Figure 3-9. Comparison of Predicted Results Using Various Cell Models For Target A in the Horizontal Direction With Test Data. Initial Bubble Velocity = 0, FL/D = 0, P_{DW} = 12.71 psi, ΔP = 0

*Proprietary information deleted

1764 078

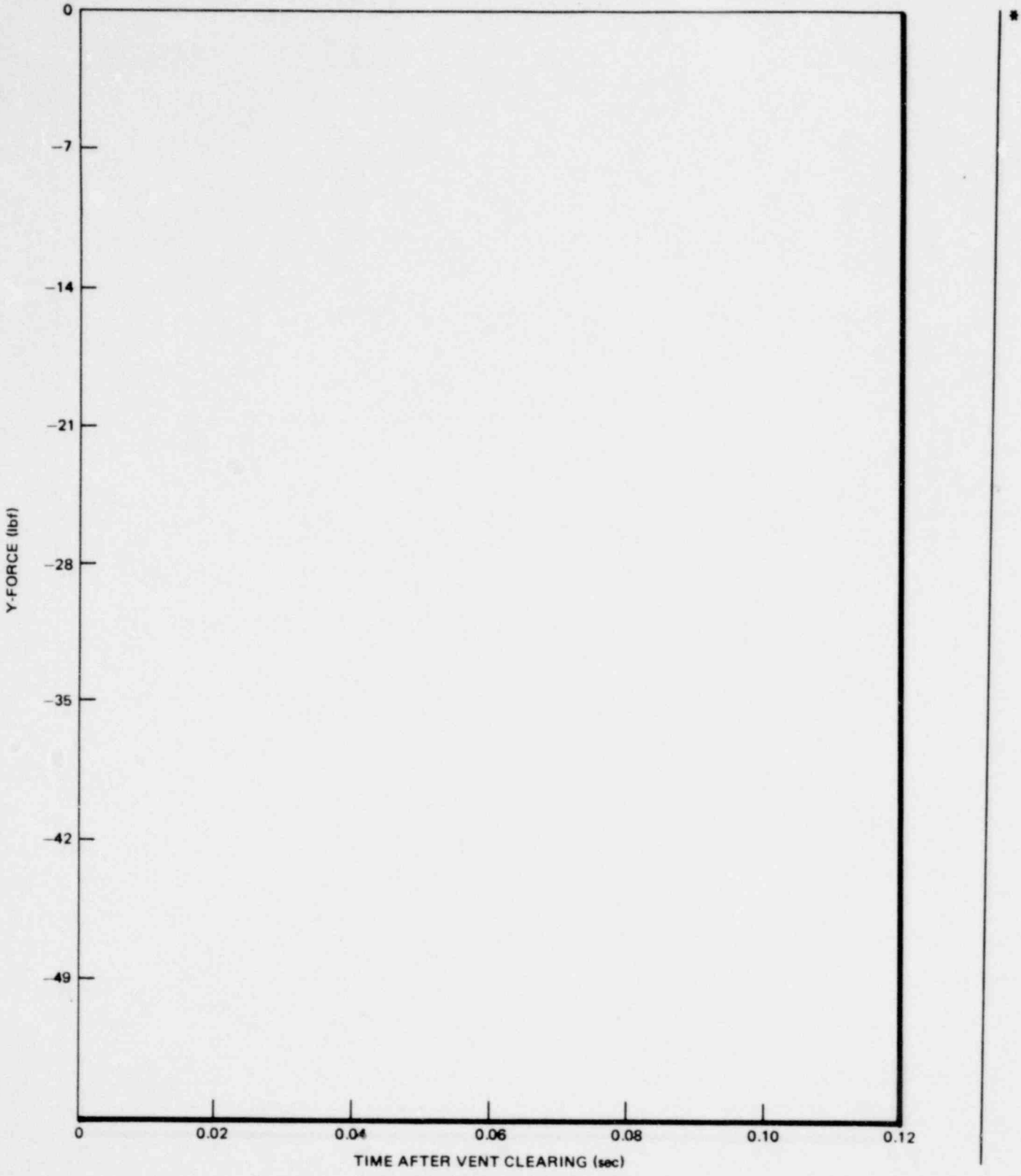

Figure 3-10. Comparison of Predicted Results Using Various Cell Models for Target B in the Vertical Direction with Test Data. Initial Bubble Velocity = 0, FL/D = 0, P_{DW} = 12.71 psi, ΔP = 0

1764 079

*Proprietary information deleted

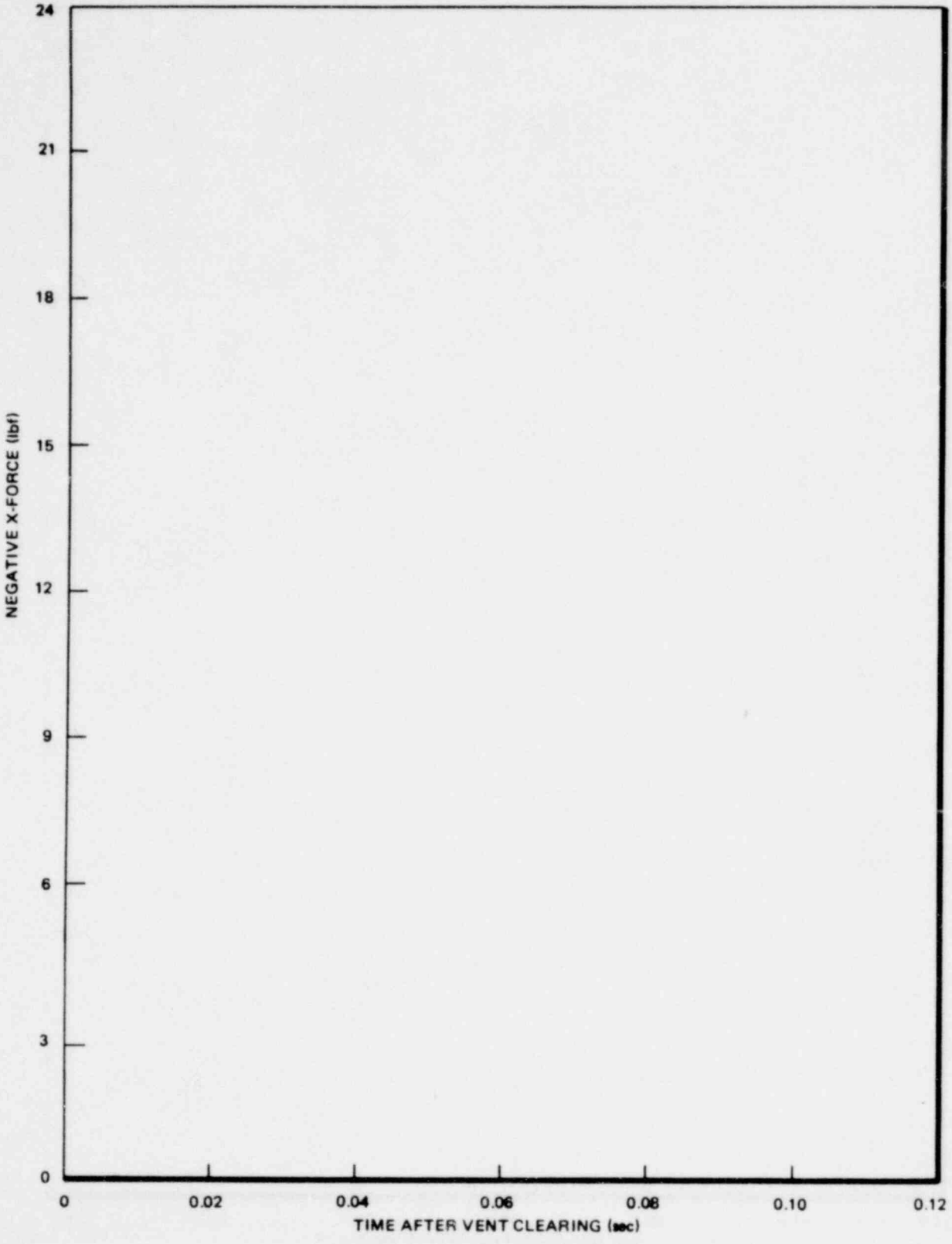

Figure 3-11. Comparison of Predicted Results Using Various Cell Models for Target B in the Horizontal Direction With Test Data. Initial Bubble Velocity = 0, FL/D = 0, P_{DW} = 12.71 psi, ΔP = 0

*Proprietary information deleted

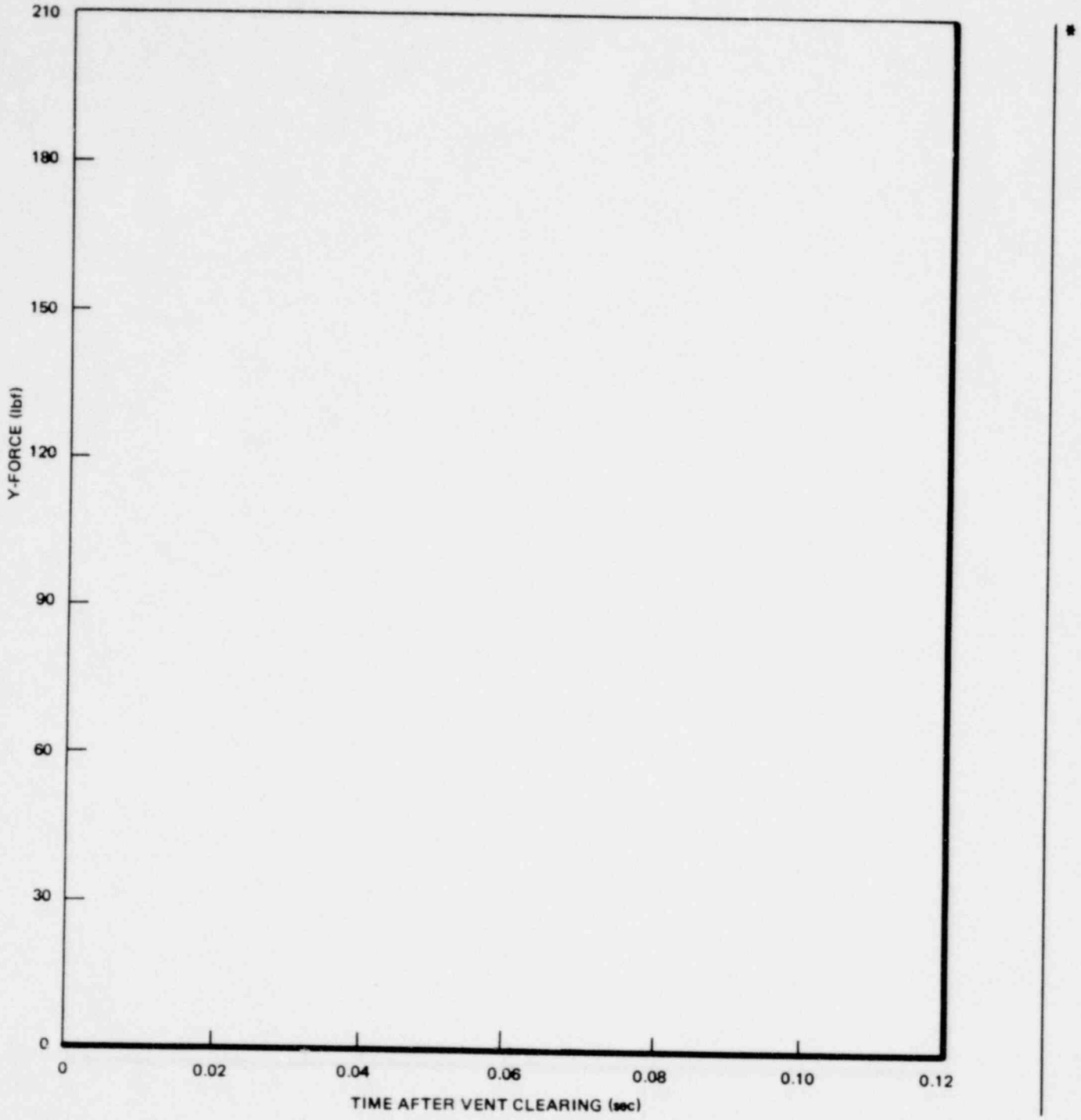

Figure 3-12. Comparison of Predicted Results Using Various Cell Models for Target C in the Vertical Direction With Test Data. Initial Bubble Velocity = 0, FL/D = 0, P_{DW} = 12.71 psi, ΔP = 0

*Proprietary information deleted

1764 081

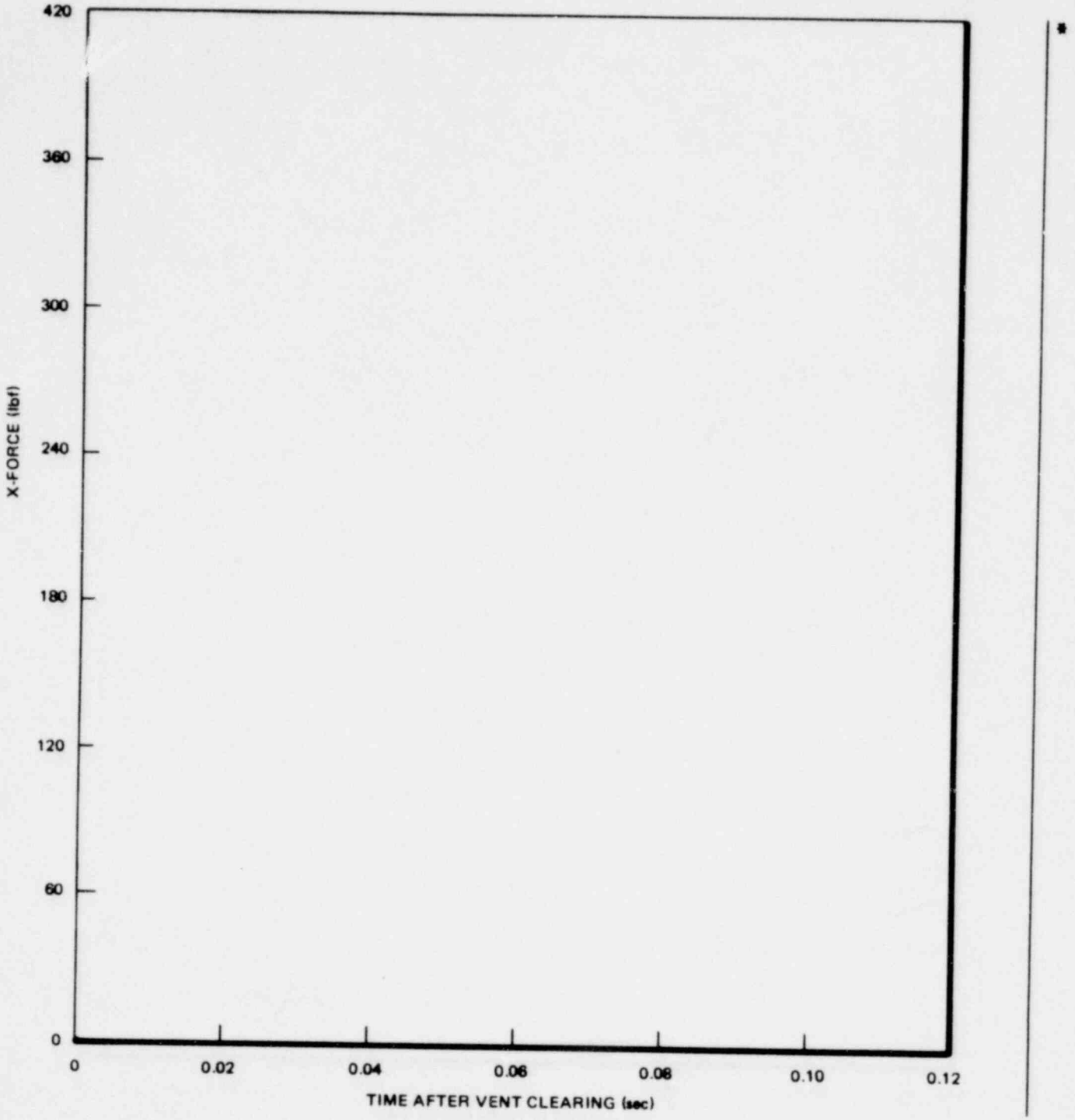

Figure 3-13. Comparison of Predicted Results Using Various Cell Models for Target C in the Horizontal Direction With Test Data. Initial Bubble Velocity = 0, FL/D = 0, P_{DW} = 12.71 psi, ΔP = 0

*Proprietary information deleted

1764 082

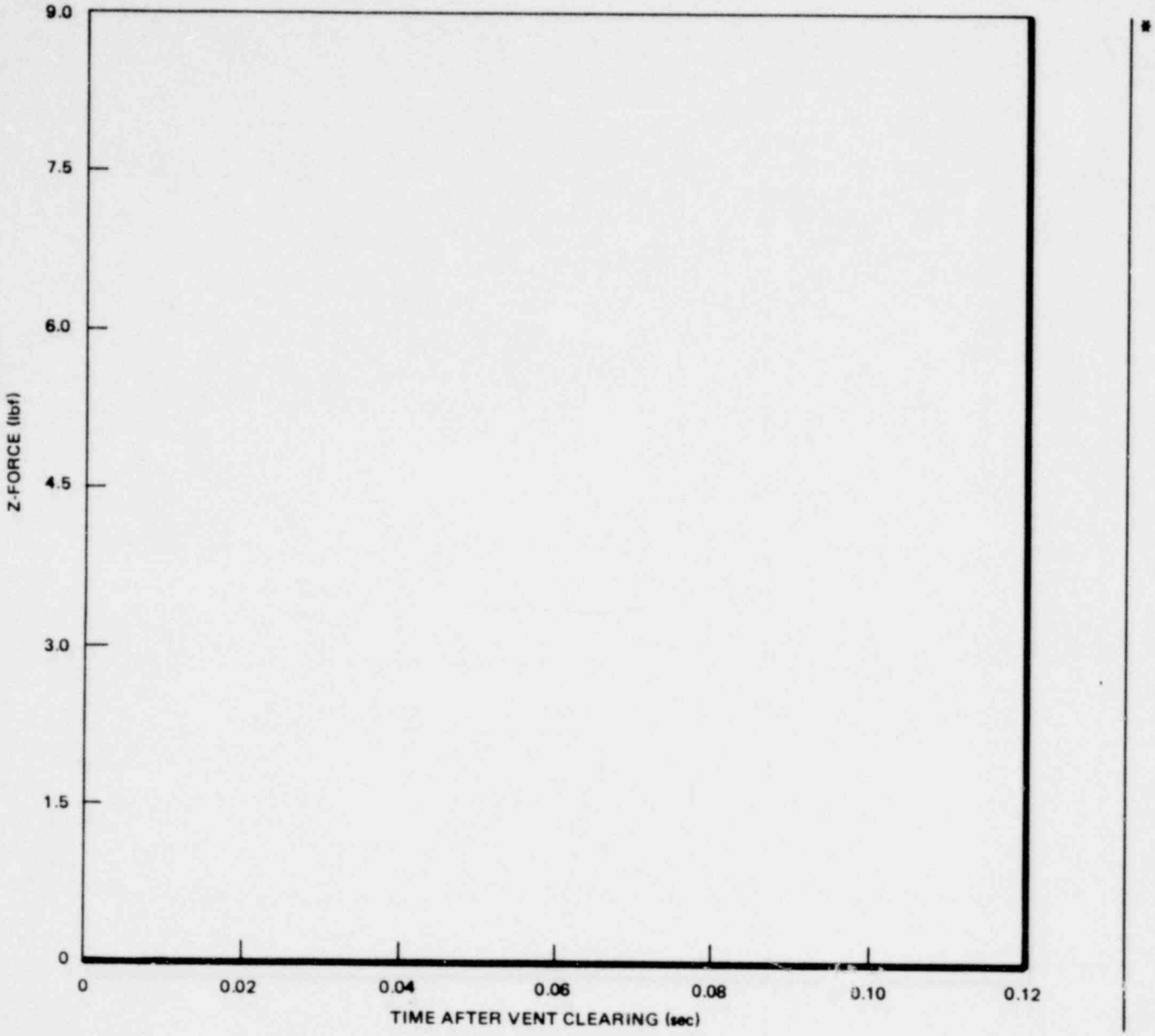

Figure 3-14. Comparison of Predicted Results Using Various Cell Models for Target D with Test Data. Initial Bubble Velocity = 0, FL/D = 0, P_{DW} = 12.71 psi, ΔP = 0

*Proprietary information deleted

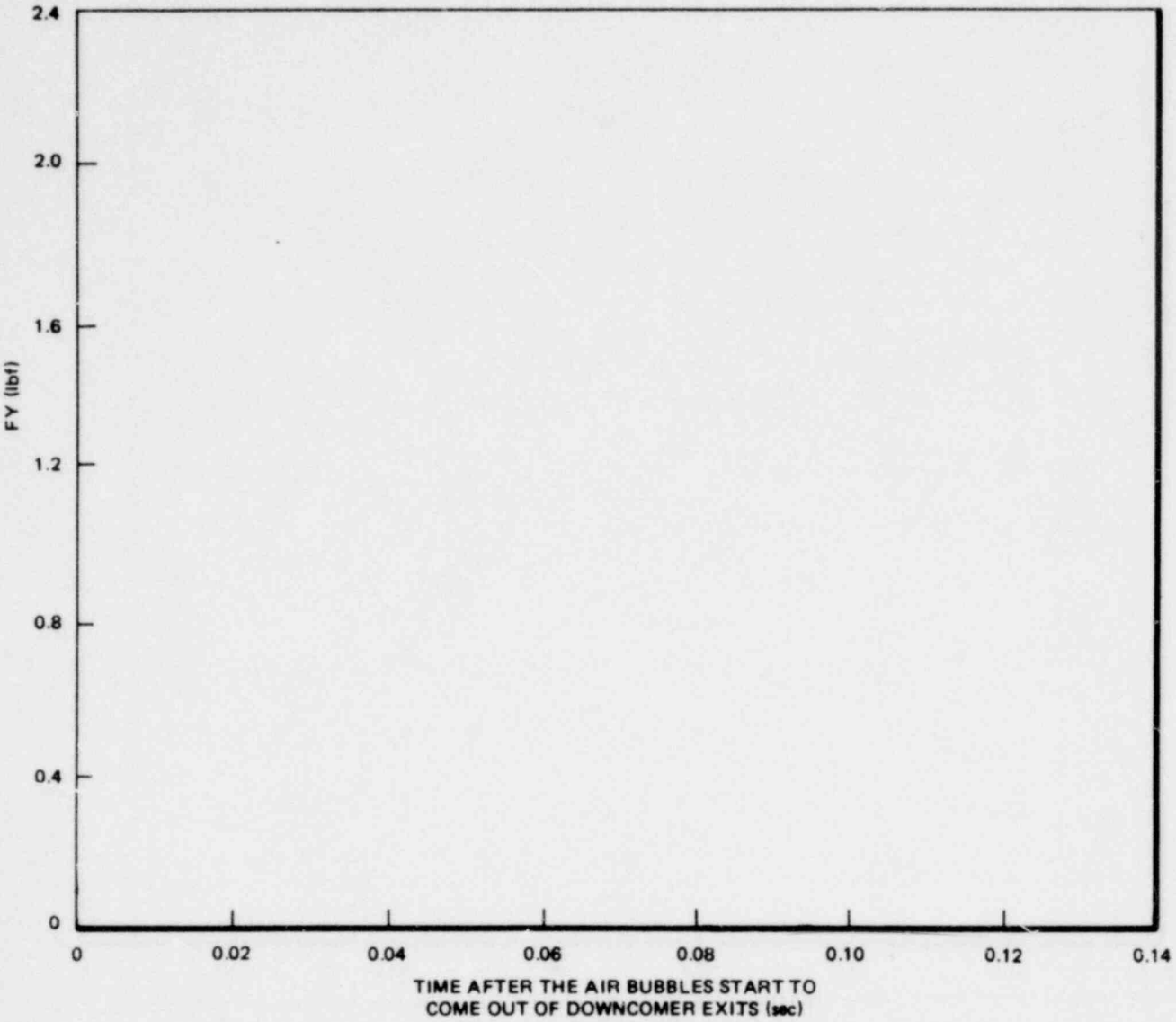

Figure 3-15. Data/Model Comparison - Target A, Vertical Force. Initial Bubble Velocity = 0 ft/sec, FL/D = 17.6, P_{DW} = Trans, Δ^{P} = 10 in.

*Proprietary information deleted

1764 084

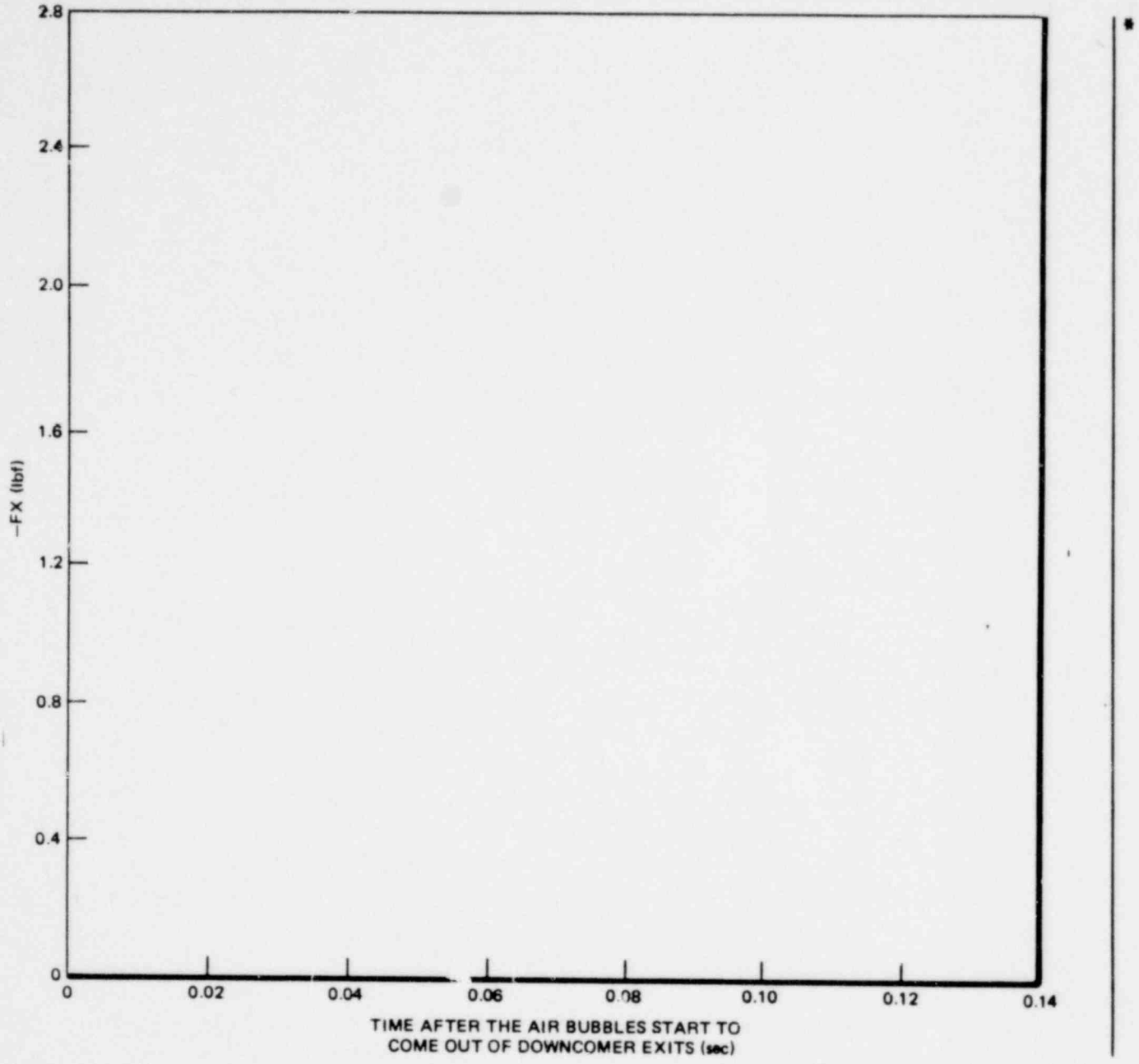

Figure 3-16. Data/Model Comparison - Target A, Horizontal Force. Initial Bubble Velocity = 0 ft/sec, FL/D = 17.6, P_{DW} = Trans, ΔP = 10 in.

*Proprietary information deleted

1764 085

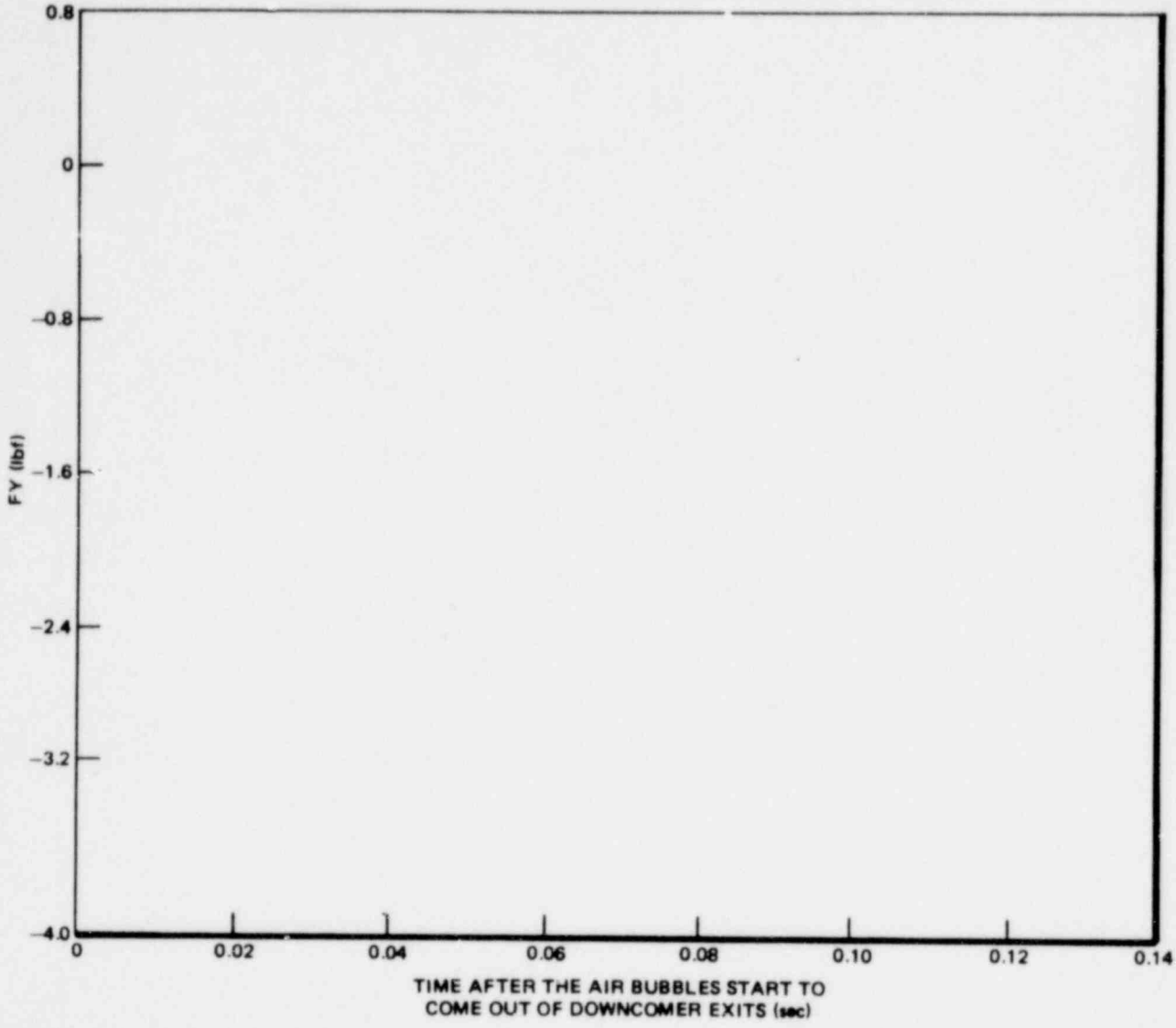

Figure 3-17. Data/Model Comparison - Target B, Vertical Force. Initial Bubble Velocity = 0 ft/sec, FL/D = 17.6, P_{DW} = Trans, ΔP = 10 in.

*Proprietary information deleted

1764 086

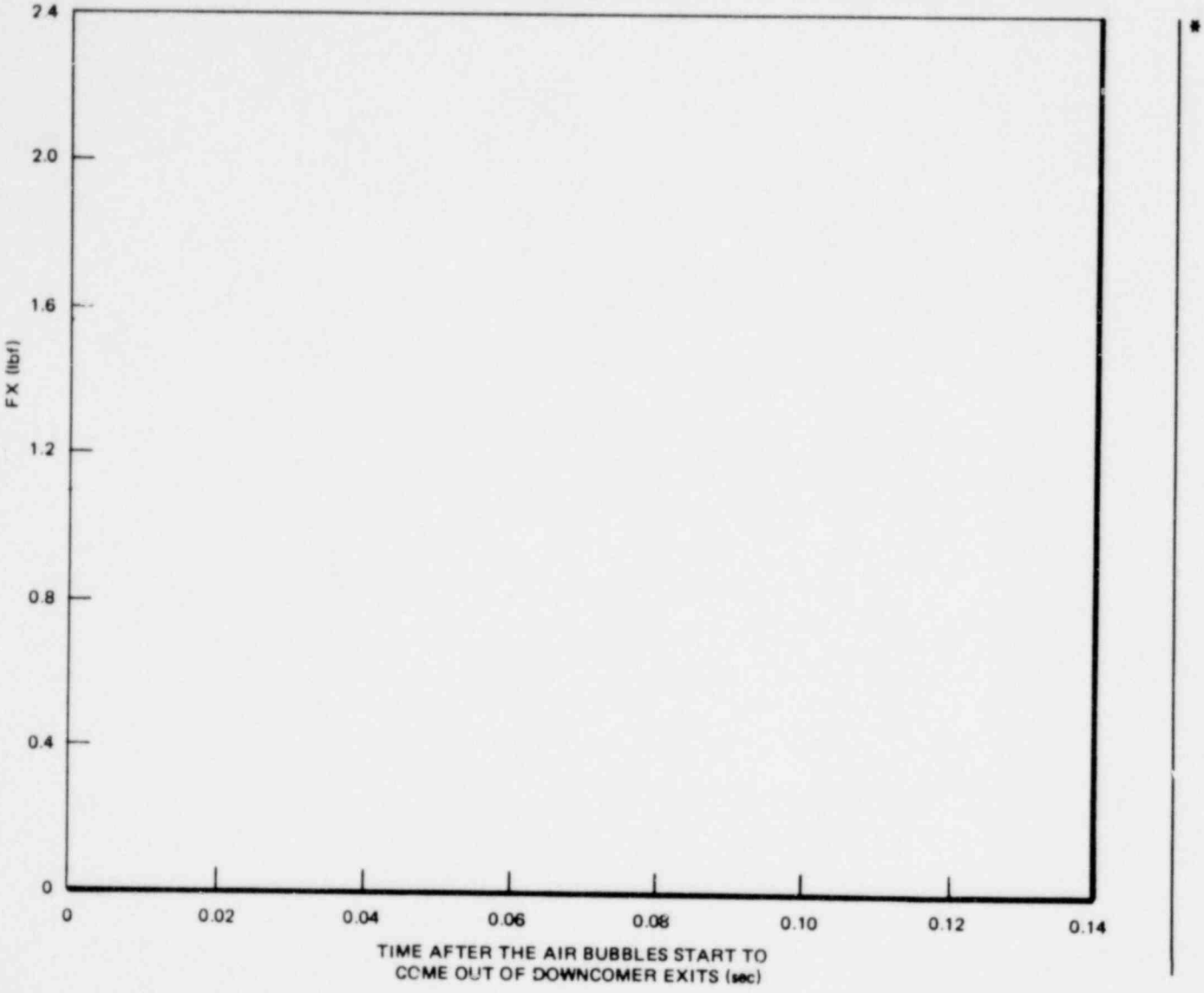

Figure 3-18. Data/Model Comparison - Target B, Horizontal Force. Initial Bubble Velocity = 0 ft/sec, FL/D = 17.6, P_{DW} = Trans, ΔP = 10 in.

*Proprietary information deleted

1764 087

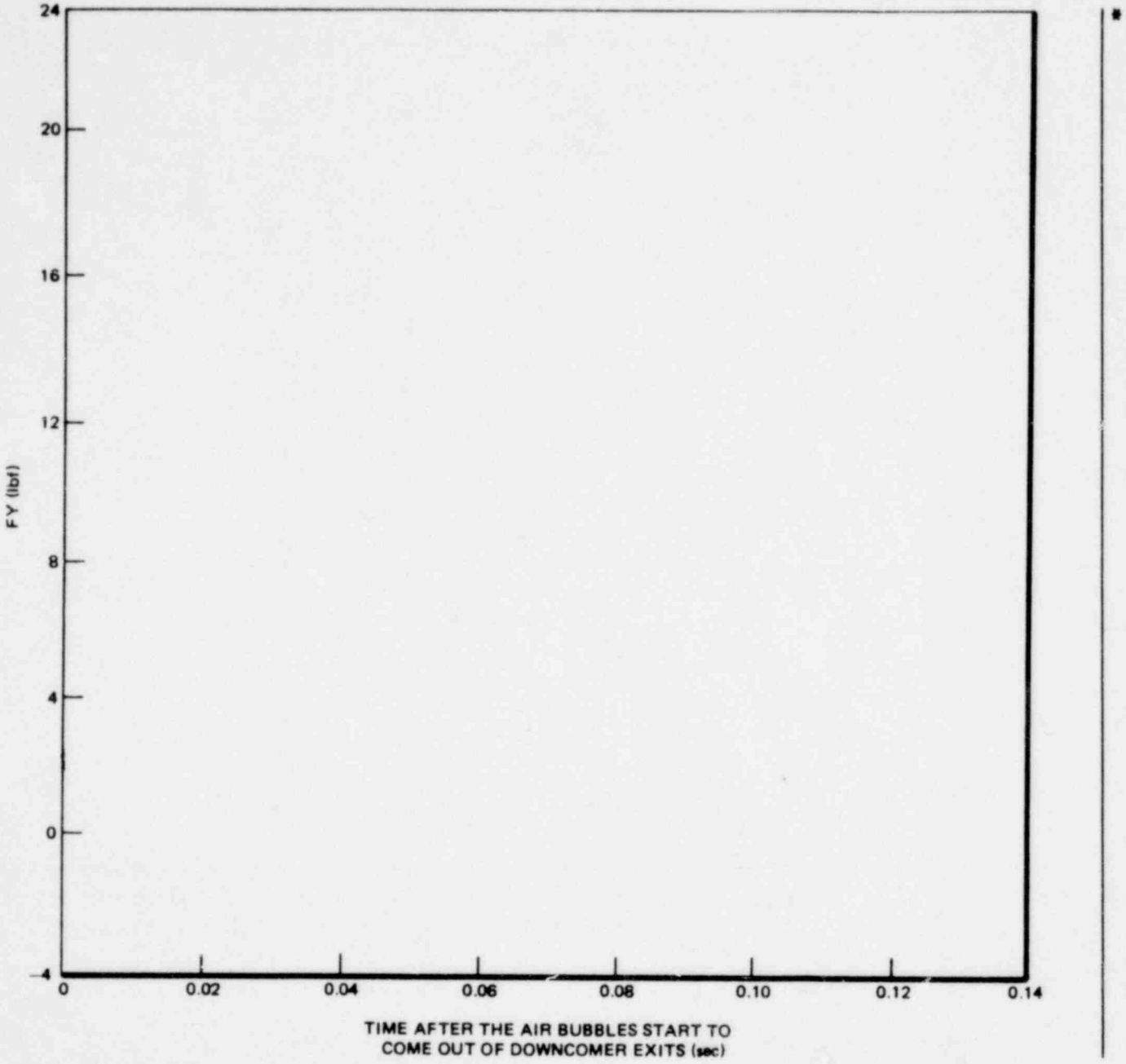

Figure 3-19. Data/Model Comparison - Target C, Vertical Force. Initial Bubble Velocity = 0 ft/sec, FL/D = 17.6, P_{DW} = Trans, ΔP = 10 in.

*Proprietary information deleted

1764 088

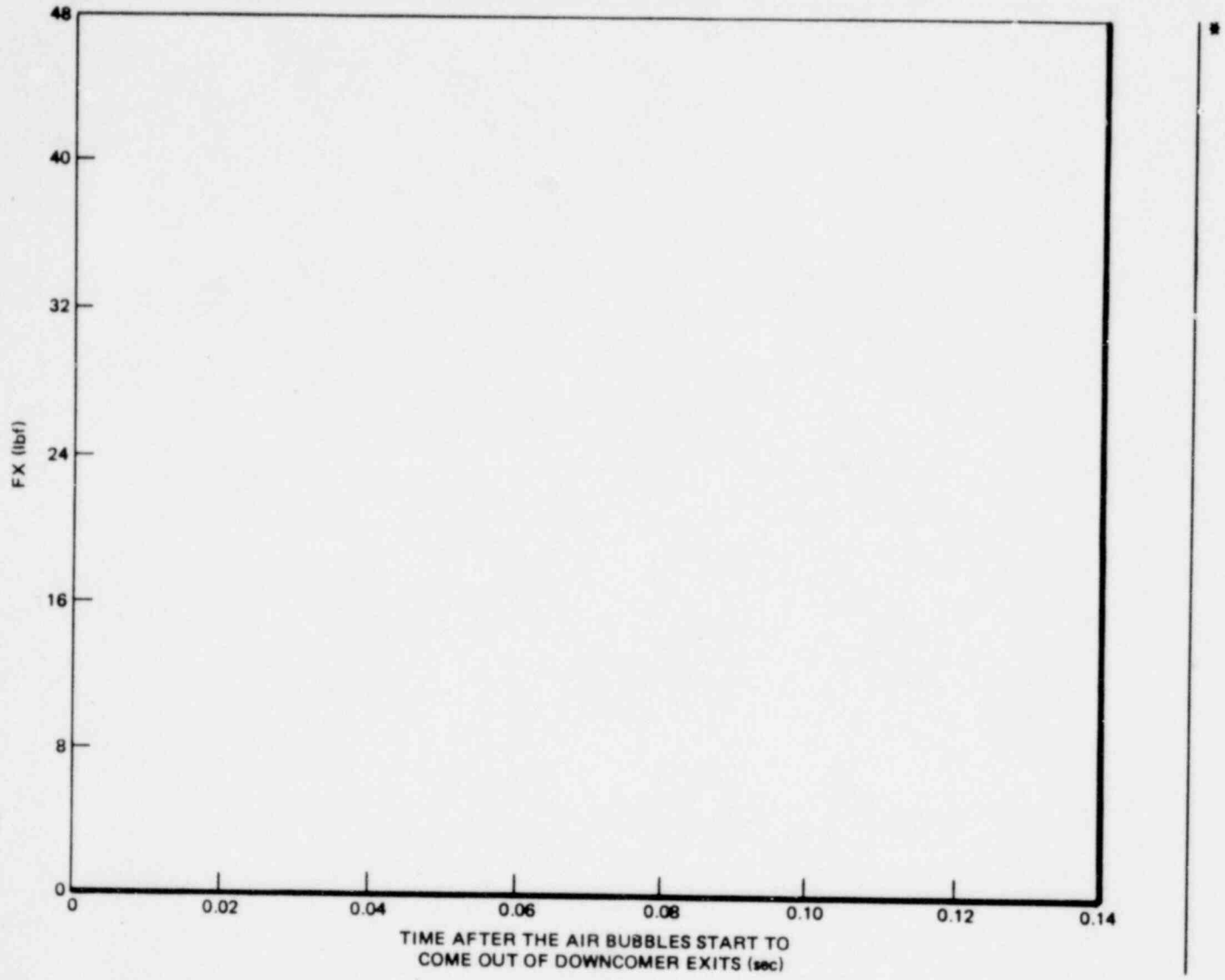

Figure 3-20. Data/Model Comparison - Target C, Horizontal Force. Initial Bubble Velocity = 0 ft/sec, FL/D = 17.6, P_{DW} = Trans, ΔP = 10 in.

*Proprietary information deleted

1764 089

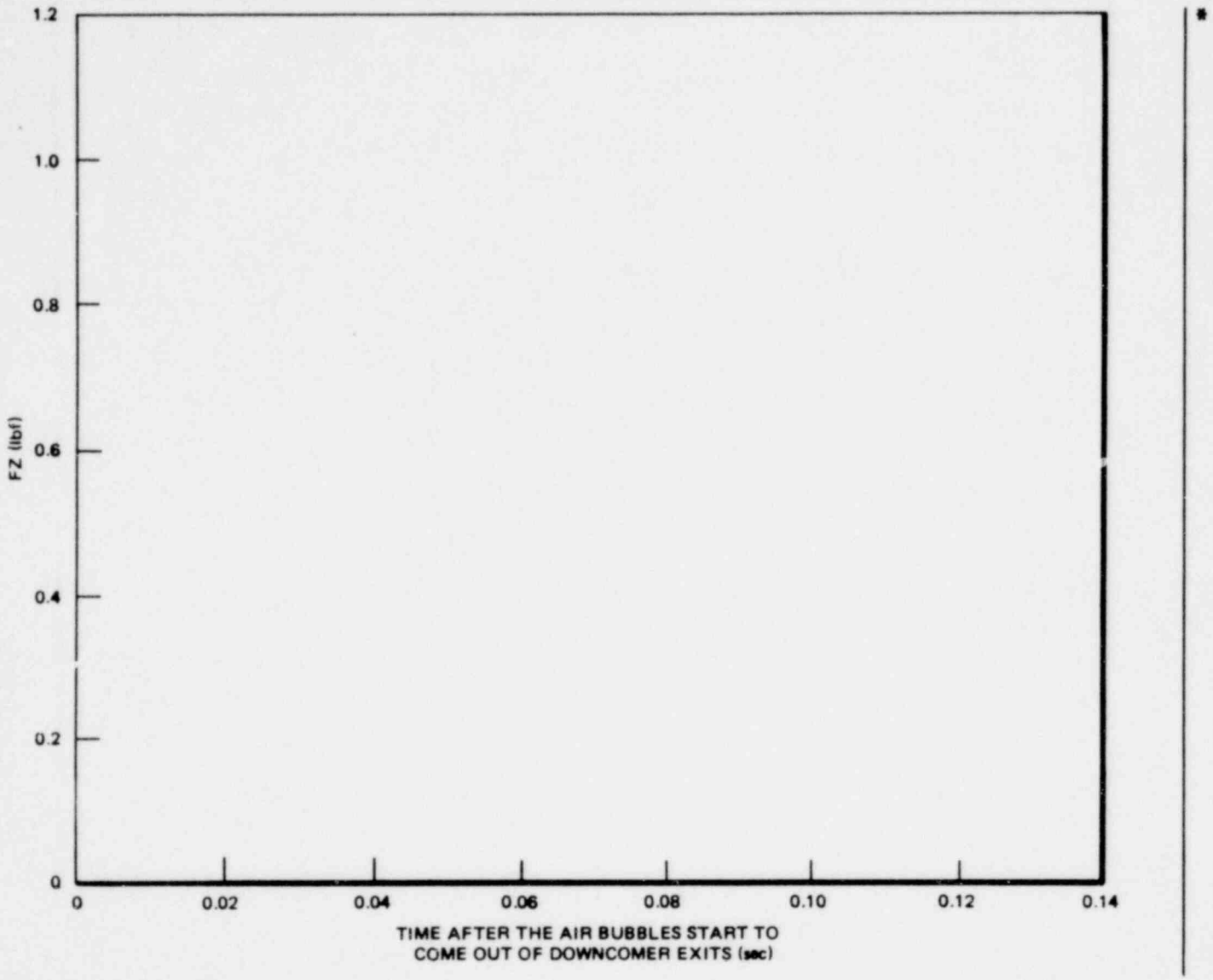

Figure 3-21. Data/Model Comparison - Target D, Horizontal Force. Initial Bubble Velocity = 0 ft/sec, FL/D = 17.6, P_{DW} = Trans, ΔP = 10 in.

1764 090

*Proprietary information deleted

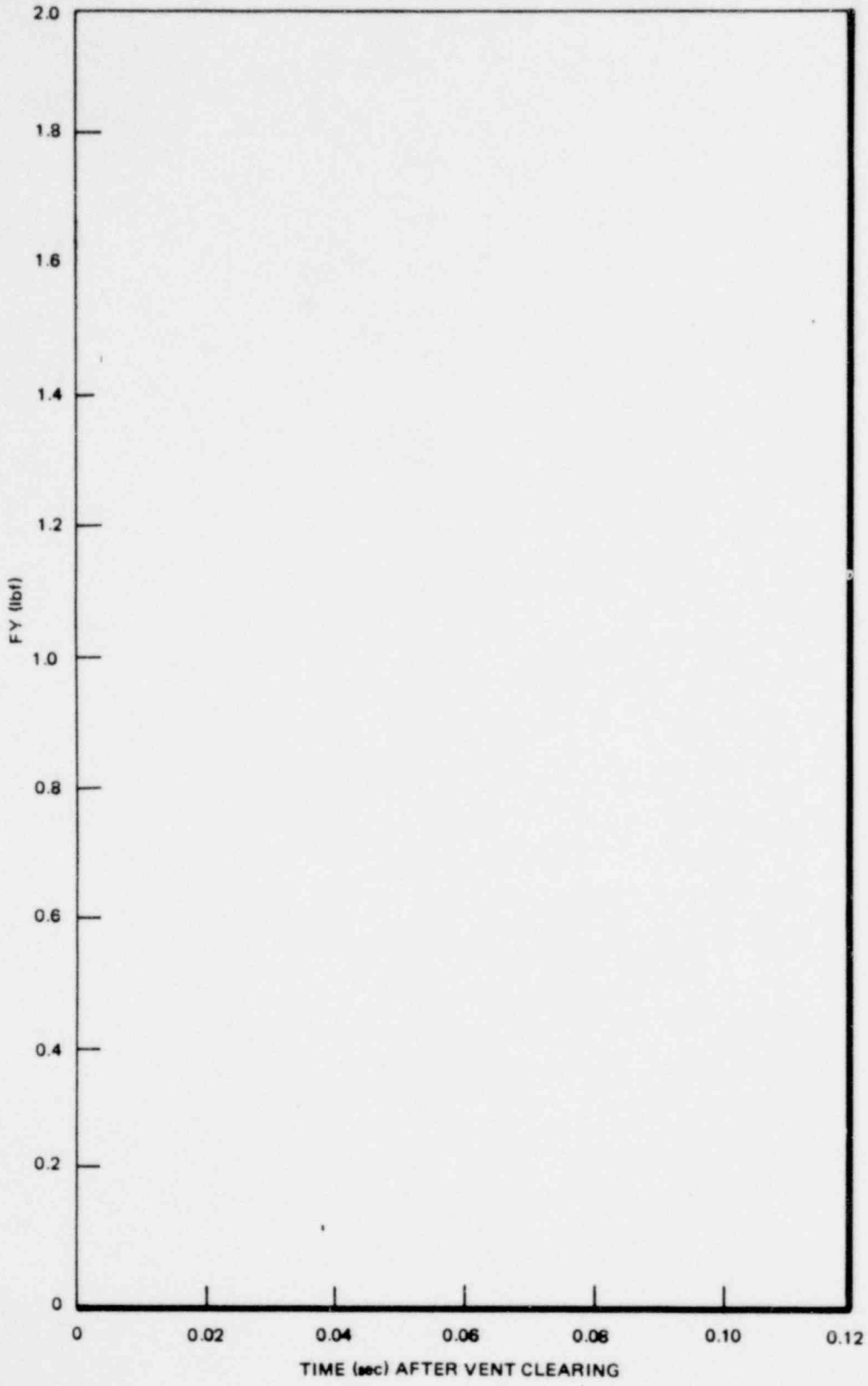

Figure 3-22. Data/Model Comparison - Target A, Vertical Force. Initial Bubble Velocity = 7.5 ft/sec, FL/D = 17.6, P_{DW} = Trans, ΔP = 0

*Proprietary information deleted

1764 091

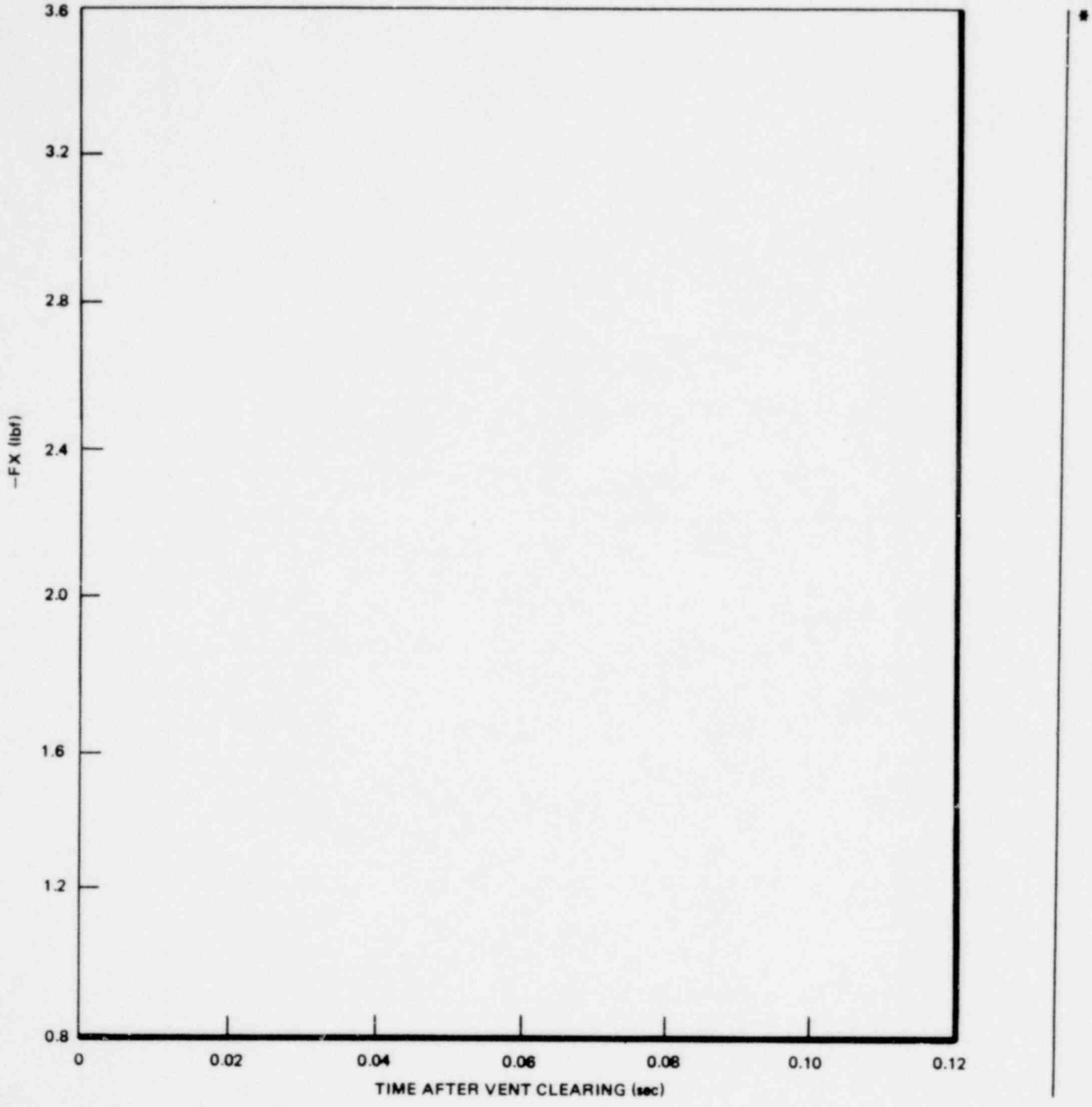

Figure 3-23. Data/Model Comparison - Target A, Horizontal Force. Initial Bubble Velocity = 7.5 ft/sec, FL/D = 17.6, P_{DW} = Trans, ΔP = 0

*Proprietary information deleted

1764 092

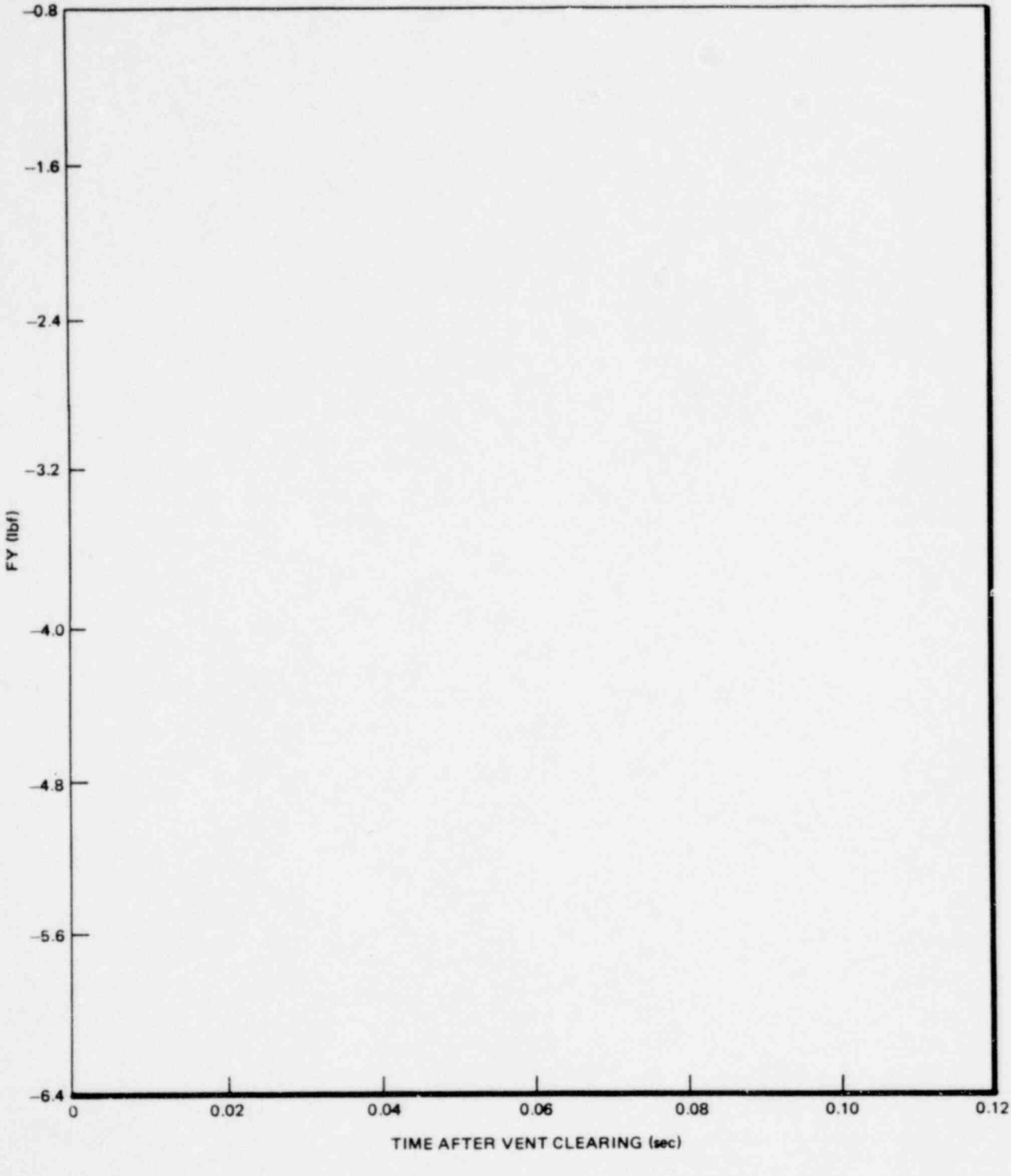

*

Figure 3-24. Data/Model Comparison - Target B, Vertical Force. Initial Bubble Velocity = 7.5 ft/sec, FL/D = 17.6, P_{DW} = Trans, ΔP = 0

*Proprietary information deleted

1764 093

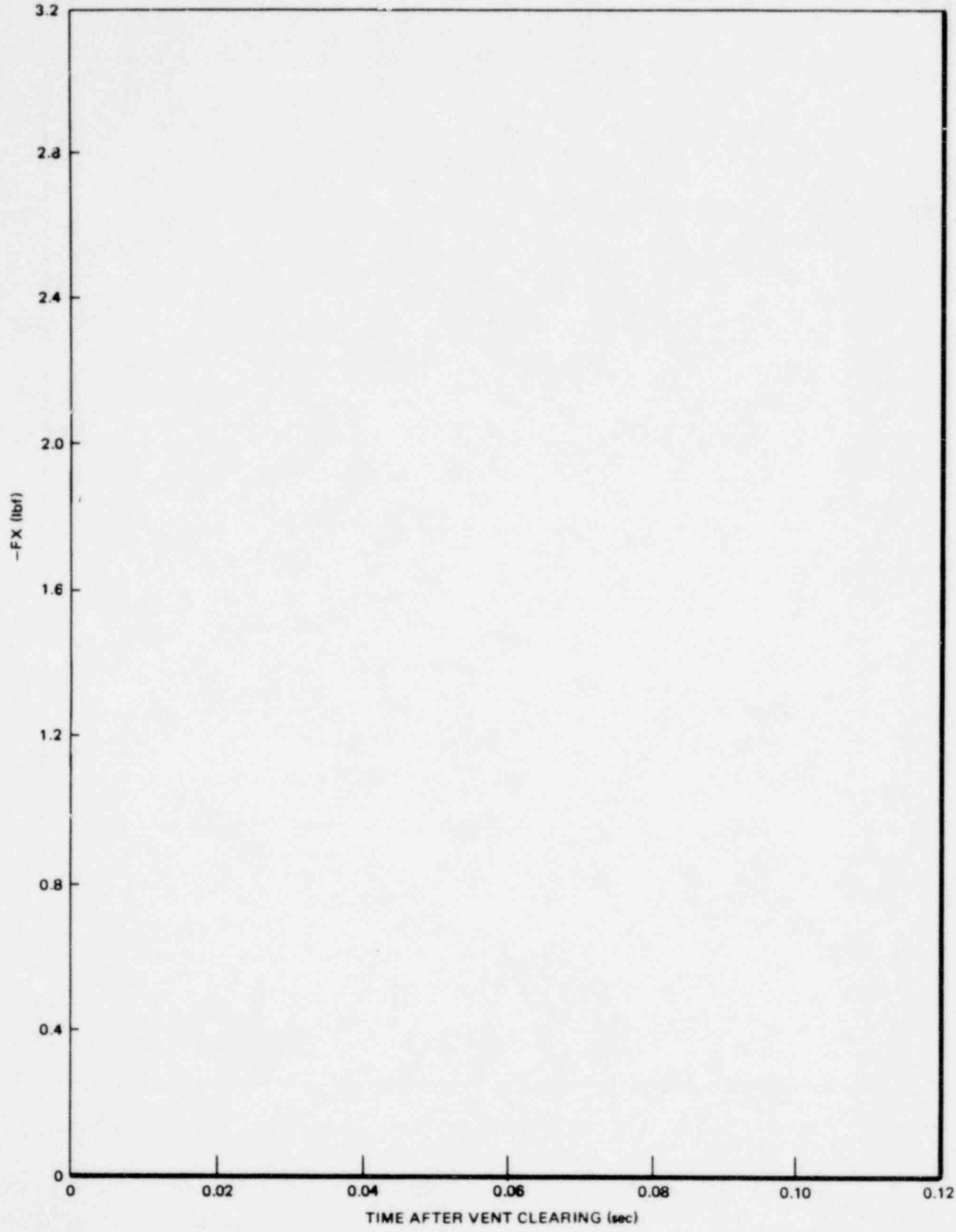

Figure 3-25. Data/Model Comparison - Target B, Horizontal Force. Initial Bubble Velocity = 7.5 ft/sec, FL/D = 17.6, P_{DW} = Trans, ΔP = 0

*Proprietary information deleted

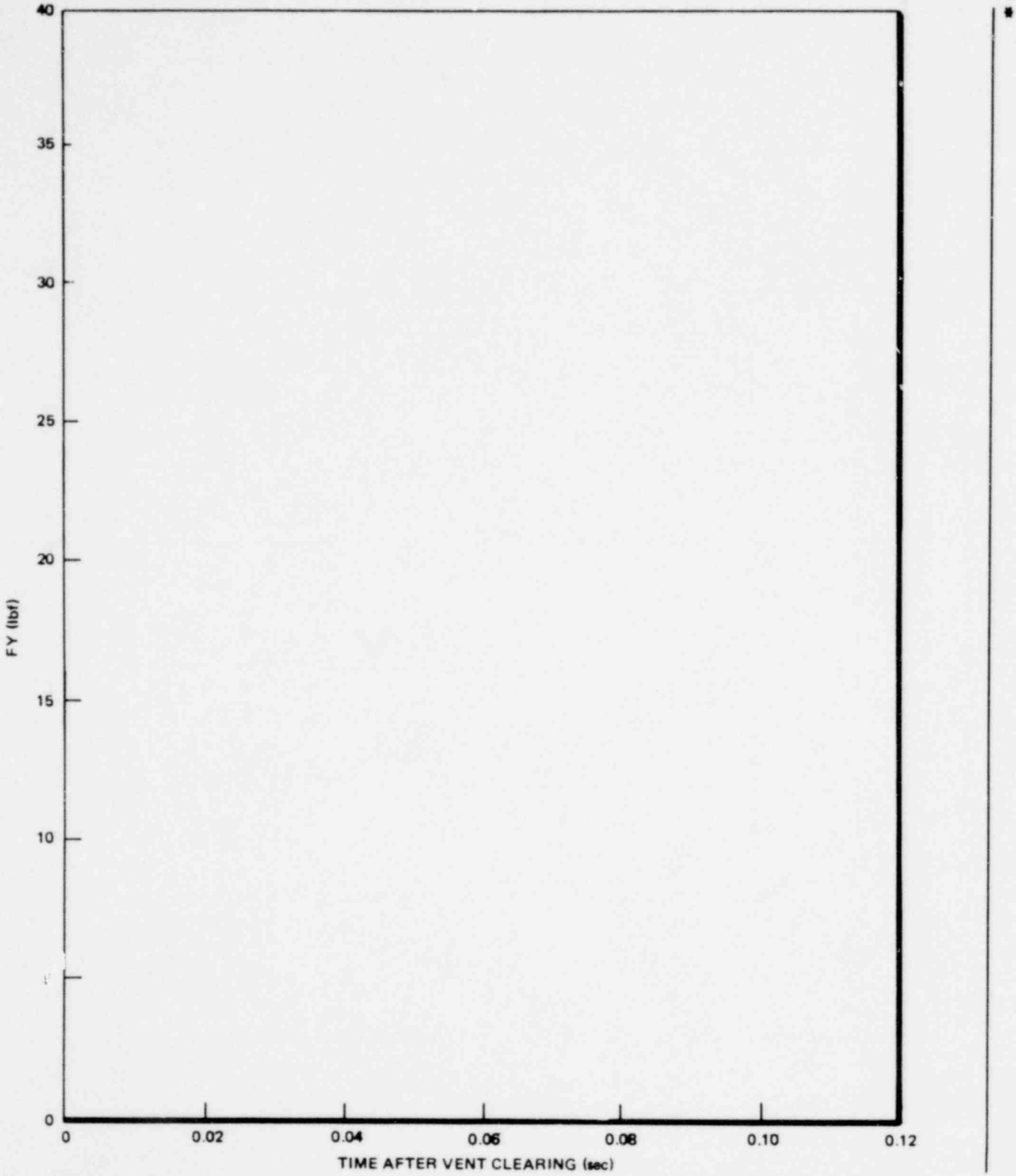

Figure 3-26. Data/Model Comparison - Target C, Vertical Force. Initial Bubble Velocity = 7.5 ft/sec, FL/D = 17.6, P_{DW} = Trans, ΔP = 0

*Proprietary information deleted

1764 095

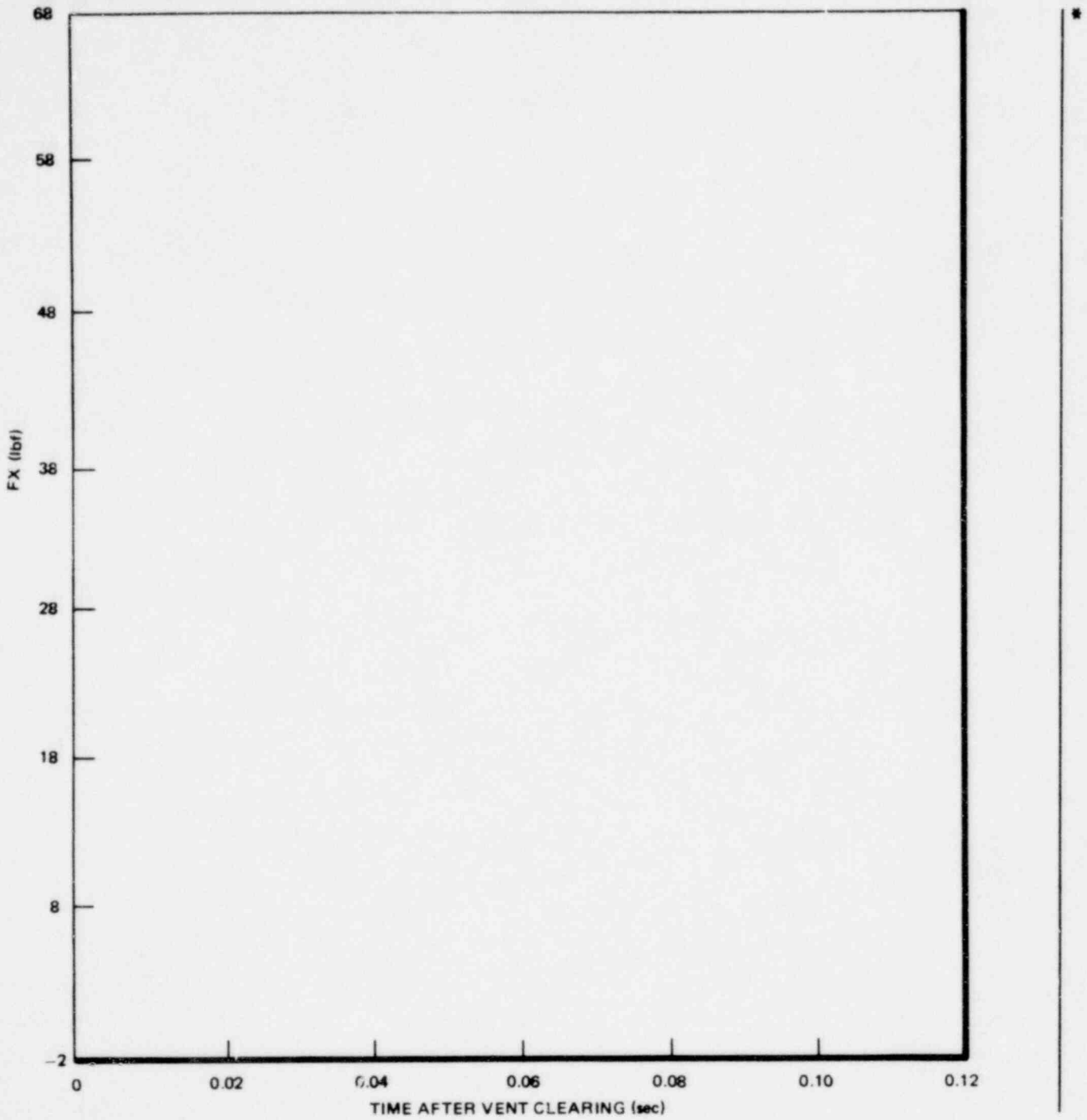

Figure 3-27. Data/Model Comparison - Target C, Horizontal Force. Initial Bubble Velocity = 7.5 ft/sec, FL/D = 17.6, P_{DW} = Trans, ΔP = 0

*Proprietary information deleted

1764 096

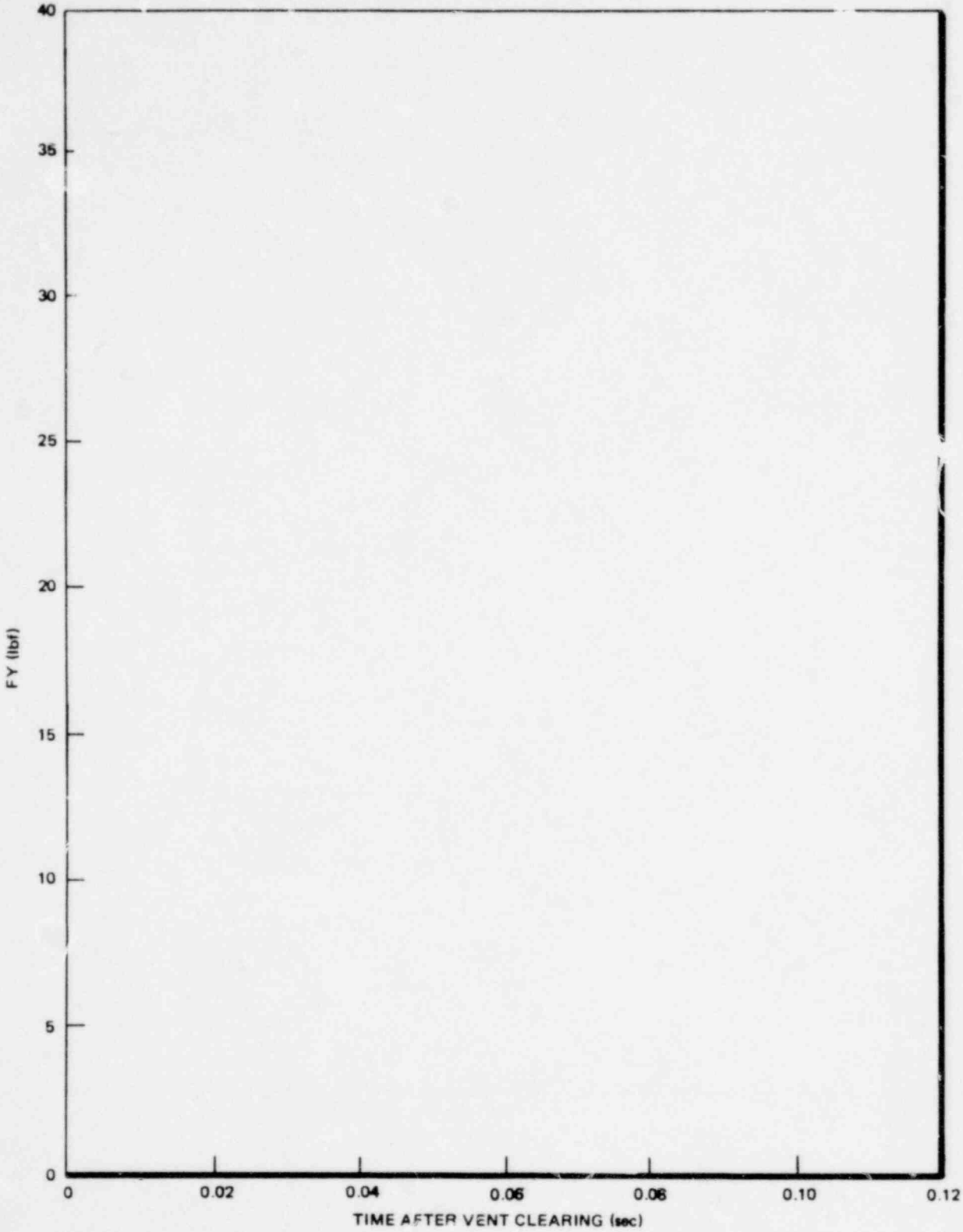

Figure 3-26. Data/Model Comparison - Target C, Vertical Force. Initial Bubble Velocity = 7.5 ft/sec, FL/D = 17.6, P_{DW} = Trans, ΔP = 0

*Proprietary information deleted

1764 097

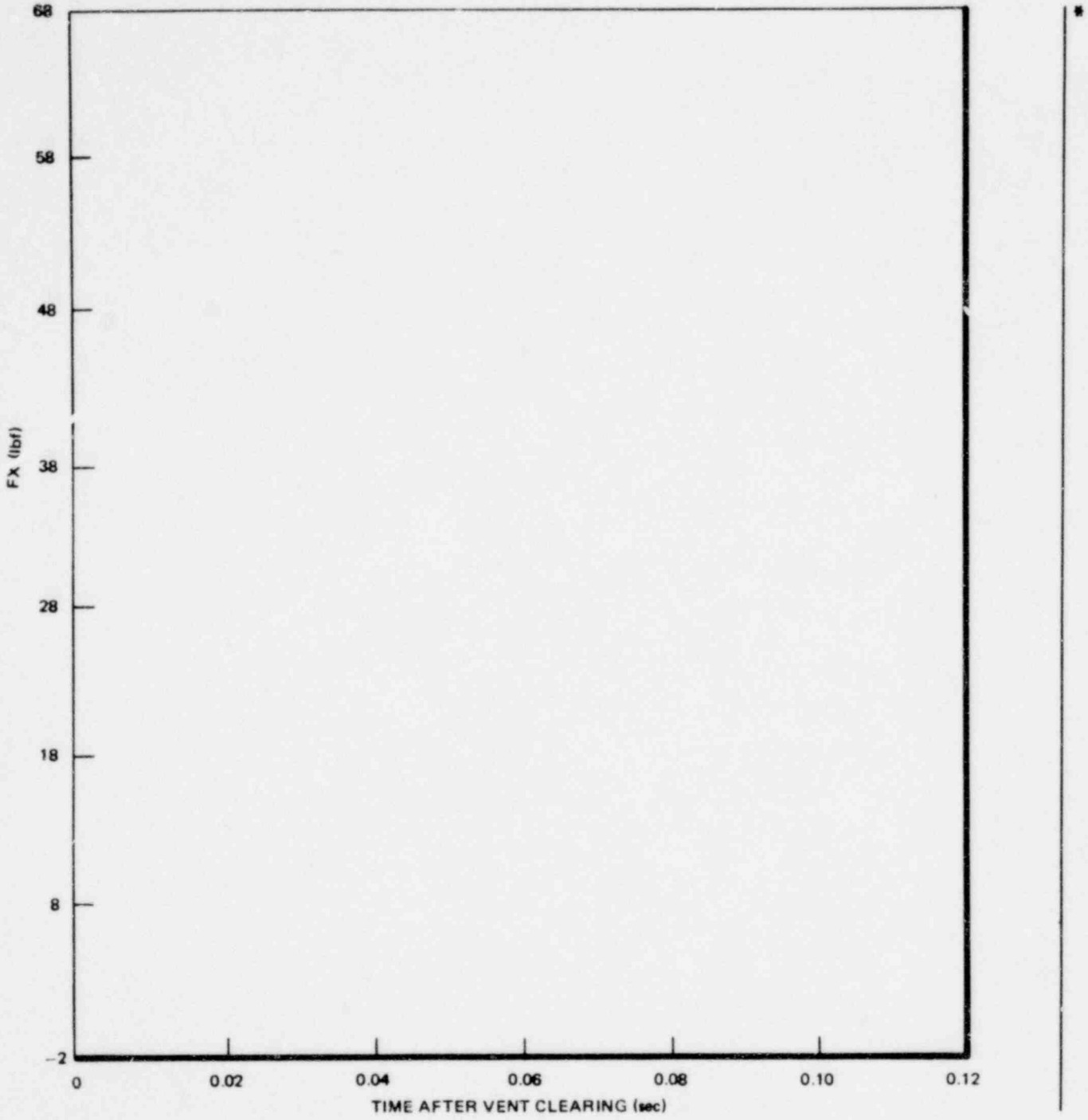

Figure 3-27. Data/Model Comparison - Target C, Horizontal Force. Initial Bubble Velocity = 7.5 ft/sec, FL/D = 17.6, P_{DW} = Trans, ΔP = 0

*Proprietary information deleted

1764 098

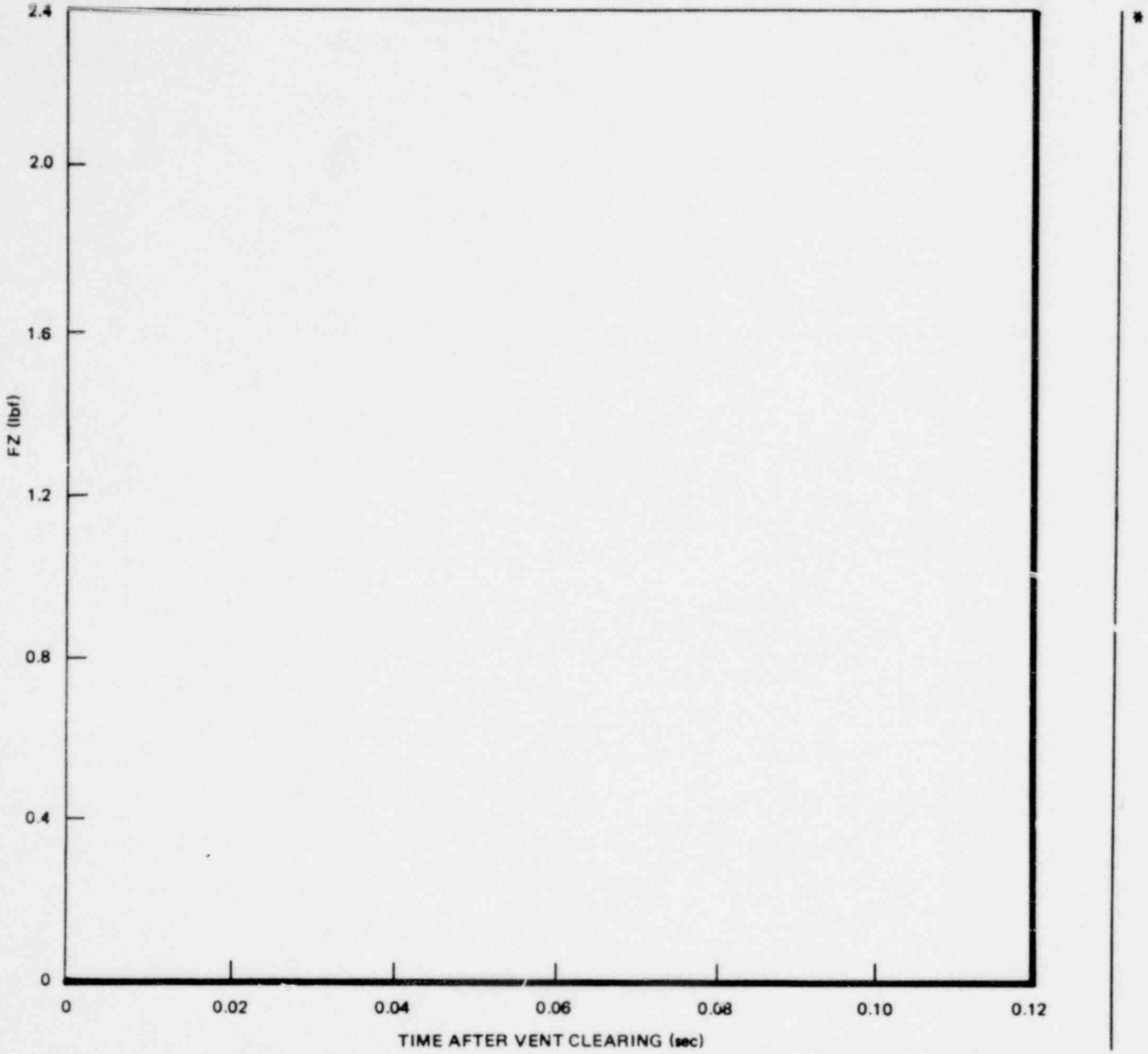

Figure 3-28. Data/Model Comparison - Target D, Horizontal Force. Initial Bubble Velocity = 7.5 ft/sec, FL/D = 17.6, P_{DW} = Trans, ΔP = 0

*Proprietary information deleted

bubble pressures) as a constant charging pressure, and with zero initial bubble wall velocity. The test data also shown in these figures is obtained from Figures 3-4 and 3-5. From these figures, the following observations are made:

1) Selection of a particular cell geometry to represent the Mark I curved boundary does affect the loads predicted on the specific target. However, all cell modelings provide the same trend of variation in target load prediction.

2) An inconsistency is observed between the model prediction and the test results. The test results show that the maximum loads on targets occur immediately after vent clearing (Figures 3-4 and 3-5). At this time in the transient, the pool is practically stagnant as observed from test films. The predominant force is therefore due to the pressure gradient (acceleration drag). The loads predicted by the analytical model, however, increase as time increases. The peak loads are predicted to occur at a later time in the transient when the bubble contacts the targets. The drag forces at this time are governed primarily by the pool velocity. Since the total drag is approximated by the sum of the acceleration drag and the standard drag ($\sim$ velocity^2), an extreme overprediction of pool velocity will cause an excessive prediction of loads on the targets. Using maximum drywell pressure before breakthrough as a constant air bubble charging pressure, zero vent friction and bubble wall velocity as input values to the analytical model tend to overpredict the pool velocity, in particular at later times in the transient. As a result of these inputs, extremely conservative loads resulted on targets as can be seen from Figures 3-8 to 3-14.

The computer program is run with consideration of vent friction, transient charging rate and initial bubble wall velocity in order to reduce the conservatism and to produce more reasonable loads. Figures 3-15 through 3-28

show comparisons between predicted results using this procedure and test data. Figures 3-15 to 3-21 provide the model/data comparisons for Targets A, B and C at ΔP = 10 in., and Figures 3-22 to 3-28 at ΔP = 10 in. The test data shown in the figures is obtained from Figures 3-4 to 3-7. From Figures 3-15 to 3-28, the following observations are made:

1) All cell modelings also provide the same trend of variation in target load prediction.

2) All predictions, with the exception of Figures 3-15 and 3-16, have shown a decreasing load at later time. This matches the actual physical loading condition observed during testing. Target A has a small diameter which in turn does not show a distinct acceleration drag load at the early time. Therefore even a small velocity may show a higher force than the acceleration drag load. It is this reason why the curves in Figures 3-15 and 3-16 do not show a drop at later time.

3) The test results, shown in Figures 3-6 and 3-7 for ΔP = 10", behave very well. The loading histories are close to the predictions.

4) It can be seen from Figures 3-15 to 3-21 that the measured peak forces under ΔP = 10 in. are bounded by the predicted peak values, although timing is later in the predictions.

5) For the case of ΔP = 0 (Figures 3-4 and 3-5), the measured loads are affected strongly by the vent clearing process. This is due to the fact that the expansion of the water column, discharged from the main vent, alters the flow pattern in the pool before the bubble enters and begins expanding. This early flow field generated by vent water clearing and followed by the flow field generated by the air bubble expansion results in fluctuating

loadings on the targets. The measured loads, therefore, do not show the same trend as those predicted by the analytical model, which does not consider the effects of the initial flow field generated by vent water clearing. Although these time histories of the test data do not agree well with the predicted values, the resultant peak forces predicted by the model for $\Delta P = 0$" still bound the peak forces obtained from test results (see Table 3-4).

From the above analysis, it is concluded that the predicted results are strongly affected by the inputs of bubble charging pressure. Inadequate input, such as use of the maximum drywell pressure before breakthrough as a constant charging pressure, will produce extremely conservative loads. The analytical approach will produce extremely conservative loads. The analytical approach should include the transient drywell pressures, the vent friction and the actual initial bubble velocity to predict more reasonable loads. When taking credit for these factors, the maximum predicted values still bound the maximum test results for the resultant forces.

Effect of Cell Modeling

Although the selection of different cell models (Table 3-3) to simulate the curved boundary does affect the load predictions in both the vertical and horizontal directions (Figures 3-8 to 3-28), the differences in the calculated resultant forces are small (Figure 3-29 as an example). This is due to the fact that the equivalent cell dimensions, when varied with respect to a specific submerged target, increase the linear dimension in one direction but reduce it in the other direction. The calculated total forces, therefore, should not vary significantly. It is demonstrated for the case of $\Delta P = 0$ (Figures 3-22 to 3-27), that although the measured peak loads in the vertical direction are somewhat higher than calculated values for some cell modeling schemes, the predicted loads in the horizontal direction are much higher than measured values (see Table 3-4). It can also be seen from Table 3-4 that the peak forces predicted for Targets A, B and C bound the total peak forces obtained from test results. The angles of resultant forces predicted by the cell models are close to the measured values.

1764 102

Table 3-4

COMPARISON OF THE MAXIMUM RESULTANT FORCES BETWEEN THE CELL MODELS PREDICTIONS AND TEST RESULTS

STRUCTURE A

Model	F_Y	F_X	F_{TOTAL}	θ	Test Results F_{total}	Test Results θ
A	1.9	2.7	3.3	35.13	2.92±0.04	34.2
B	1.60	3.4	3.75	25.29		
C	1.72	3.08	3.52	29.18		
D	1.605	3.3	3.67	29.94		
E	1.55	3.45	3.78	24.19		

STRUCTURE B

Model	F_Y	F_X	F_{TOTAL}	θ	Test Results F_{total}	Test Results θ
A	-4.86	1.94	5.23	-68.23	4.37±0.35	-59.2
B	-5.57	2.93	6.29	-62.25		
C	-5.47	2.43	5.99	-66.05		
D	-6.00	2.55	6.52	-66.97		
E	-6.25	2.69	6.80	-66.71		

STRUCTURE C

Model	F_Y	F_X	F_{TOTAL}	θ	Test Results F_{total}	Test Results θ
A	36.6	52.6	64.09	34.83	61.74±2.87	38.3
B	29.6	62.8	69.42	25.23		
C	32.8	58.4	66.98	29.32		
D	29.9	61.3	68.20	26.00		
E	28.5	63.2	69.33	24.27		

1764 103

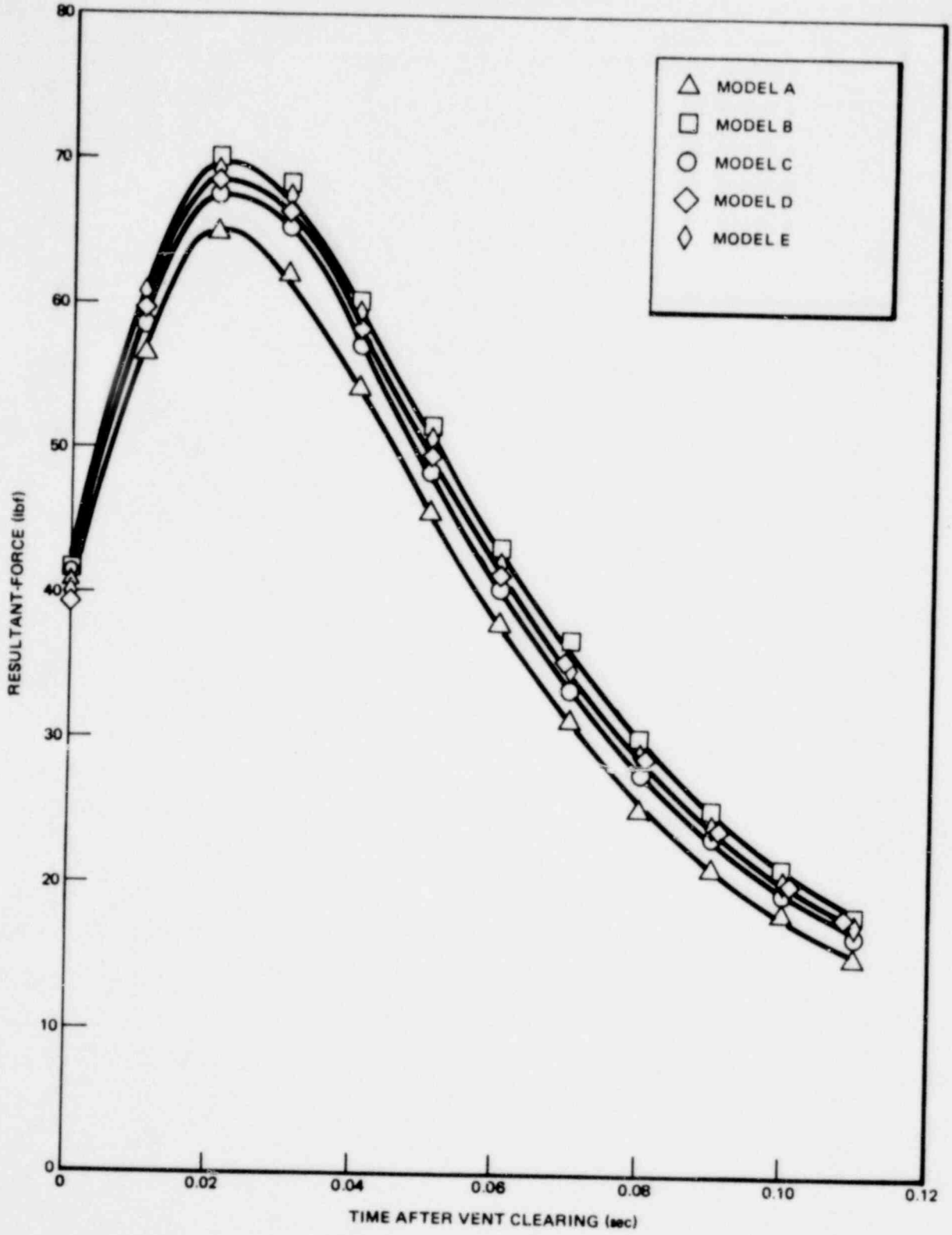

Figure 3-29. Predicted Resultant Forces Using Various Cell Models for Target C. Initiate Bubble Velocity = 7.5 ft/sec, FL/D = 17.5, P_{DW} = Trans

1764 104

Verification of Uniform Flow Assumption

In addition to the load comparison between predicted and measured values, confirming the validity of the uniform flow assumption made in the model was also one of the main objectives. In order to meet this objective, targets A and C were positioned at equal distances from the center of the bubble. To satisfy the uniform flow assumption, in this case, the ratio of the measured acceleration predominated drag forces on Target C to those on A should be equal to the ratio of the target hydrodynamic volumes (a numerical value of $(D_C/D_A)^2$ since targets are cylindrical and target lengths are the same).

Since the peak drag forces are dominated by acceleration drag rather than standard drag (Figures 3-4 to 3-7), these peak forces for Targets A and C should be predominantly a function of the acceleration volume, and can be employed for validation of the uniform flow assumption. It is found from the test results (Table 3-1), that the ratio of measured resultant force of Targets C and A is $(4.6)^2$ for ΔP = 10 in. and $(4.4)^2$ for ΔP = 0 in. These two ratios compare favorably to the ratio of the respective diameters squared, $(D_C/D_A)^2 = (4.8)^2$. The test results, therefore, confirm the validity of the uniform flow assumption for the computation of acceleration drag.

Loads on the Vertical Target

Model/data comparison for Target D is presented in Figure 3-28. It can be seen from this figure that the predicted values with different cell models bound the measured results given in Table 3-2. It should be noted that the loads shown in the Table 3-2 are computed considering the peak force, measured at one location on the Target D, to act over the entire target as a bounding value.

Effects of Drywell Initial Overpressure

The effects of full drywell initial overpressure on submerged target loads (i.e., $\Delta P = 10"$) are shown in Table 3-1. The average peak force per unit area with $\Delta P = 10"$ is approximately 40% of the peak with $\Delta P = 0"$. This is due to a lower charging pressure in the case of $\Delta P = 10"$ than in $\Delta P = 0"$. This can be seen from the bubble pressure trace shown in Figure 3-6.

Effects of Pool Swell and Fall Back Events

There is no significant measured load for any of the targets during the consequent velocity dominated phase of the pool swell and fall back events. It is concluded that the hydrodynamic loads on structures submerged below the main vent exit (Targets A, B and C) can be neglected during the pool swell and the fall back events.

4. CONCLUSIONS

The one-quarter scale Mark I submerged structure test program was devised to verify proposed analytical model for predicting loads on submerged structures caused by the flow fields generated by a postulated LOCA air discharge.

The following conclusions can be drawn:

1. In general, the forces measured on the Mark I 1/4 scale test targets are small. For the large target (Target C, 6" in diameter), the average peak force per unit area is slightly over 1 psi. For all the runs with ΔP = 10", the average peak force per unit area is approximately 40% of the peak with ΔP = 0 (Table 3.1).

2. The ratio of measured resultant force (1/4 scale test) of Target C to A is $(4.6)^2$ for ΔP = 10 in. and $(4.4)^2$ for ΔP = 0. Since the peak force is predominantly due to acceleration drag, with the assumption that the flow field is uniform, the ratio of the force for two targets that are located symmetrically in the flow field is proportional to the ratio of their respective diameters squared. The ratio of the respective diameters between these two targets is equal to 4.8 which compares favorably to the measured ratios of 4.6 and 4.4. This agreement shows the validity of the assumption of a uniform flow field.

3. From model/data comparisons of the 1/4 scale test, it is found that the predicted loads are grossly conservative if constant maximum driving pressure (major assumption 6, Section 2.1), zero vent friction and bubble wall velocity are applied. Even after including all corrected factors, i.e., the transient bubble pressure, vent friction and actual initial bubble velocity, the predicted values still conservatively bound the test results of the resultant force. It is concluded that to predict reasonable bubble loads, the corrected factors should be used to reduce the conservatism of the original analytical approach.

4. Variation of geometric call parameters over a wide range of conditions to represent the curved pool boundary resulted in only minor variation of calculated submerged structural forces. Thus it is concluded that pool shape parameters are of secondary importance in predicting resultant forces on submerged structures.

5. There is no significant measured load on targets below the main vent exit during the consequent velocity dominated phase of the pool swell and fall back events.

5. REFERENCES

1. F. J. Moody, L. C. Chow, and L. E. Lasher, "Analytical Model for Estimating Drag Forces on Rigid Submerged Structures Caused by LOCA and Safety/Relief Valve Ramshead Air Discharges," NEDO-21471, September 1977.

2. H. Lamb, 1932, Hydrodynamics, Dover.

3. Nuclear Services Corporation, "1/4 Scale Test Report - Loads on Submerged Structures Due to LOCA Air Bubbles and Water Jets," NEDO-23817, (to be published).

NUCLEAR ENERGY DIVISIONS • GENERAL ELECTRIC COMPANY
SAN JOSE, CALIFORNIA 95125

GENERAL ELECTRIC

TECHNICAL INFORMATION EXCHANGE

TITLE PAGE

AUTHOR	SUBJECT	TIE NUMBER
S. L. Liu and L. E. Lasher	Reactor Technology	79NED79
		DATE September 1979
TITLE: Submerged Structures Model Main Vent Air Discharges Evaluation Report		GE CLASS: I
		GOVERNMENT CLASS:
REPRODUCIBLE COPY FILED AT TECHNICAL SUPPORT SERVICES, R&UO, SAN JOSE, CALIFORNIA 95125 (Mail Code 211)		NUMBER OF PAGES: 61

SUMMARY

Predictions of the analytical model for estimating drag loads on submerged structures by main vent air discharges following a postulated loss-of-coolant accident are compared to the results obtained from the one-quarter scale Mark I submerged structure test program.

Results of the one-quarter scale Mark I submerged structure experiment show that the analytical model grossly overpredicts loads in a scaled prototypical Mark I facility. Alternate modeling is evaluated which gives more reasonable, but still conservative predictions. The quarter-scale experiment also verifies the uniform flow assumption of the analytical model.

By cutting out this rectangle and folding in half, the above information can be fitted into a standard card file.

DOCUMENT NUMBER NEDO-21983

INFORMATION PREPARED FOR Nuclear Power Systems Division

SECTION Containment Improvement Programs

BUILDING AND ROOM NUMBER PYD 409 MAIL CODE 905

GENERAL ELECTRIC